APW-LCAO band model for A15 compounds

L. F. Mattheiss

Bell Laboratories, Murray Hill, New Jersey 07974

(Received 28 April 1975)

The results of nonrelativistic augmented-plane-wave (APW) band-structure calculations at symmetry points in the cubic Brillouin zone for V_3Si, V_3Ge, Nb_3Al, and Nb_3Sn are fit using the Slater-Koster linear-combination-of-atomic-orbitals (LCAO) interpolation scheme. This LCAO model involves Bloch sums formed from 30 A-atom ($A = $ V,Nb) d orbitals and eight B-atom ($B = $ Si,Ge,Al,Sn) s-p orbitals. In its simplest form, this LCAO model fits 73 APW energy eigenvalues at Γ, X, M, and R with an rms error of 0.020–0.023 Ry by means of 21 two-center parameters. Improved accuracy is achieved, particularly for states near E_F, by weighting these more heavily in the LCAO fit, partially relaxing the two-center approximation, and increasing the number of LCAO parameters to 39. The results of this APW-LCAO model are applied to evaluate the accuracy of the Labbé-Friedel (LF) linear-chain and the Weger-Goldberg (WG) coupled-chain band models for the A15 compounds. It is concluded that (a) corrections to the LF and WG models (about 3 and 1 eV, respectively) are sufficient to wash out fine structure in the density of states on a meV energy scale; (b) there is no evidence for describing the electronic structure of these A15 as one-dimensional or quasi-one-dimensional in character; (c) the density-of-states peak near E_F involves primarily A-atom d states with $\delta_1(x^2-y^2)$ symmetry, in contrast to the predictions of the LF ($\delta_1+\delta_2$) and WG (δ_2) models; (d) the accuracy of the present LCAO model is insufficient for predicting the precise shape of the density of states near E_F from first principles.

I. INTRODUCTION

The intermetallic A_3B compounds with the A15 or β-tungsten structure have been the subject of widespread interest because they include materials with the highest superconducting transition temperatures known. In addition, these materials frequently possess anomalies in their electrical, magnetic, elastic, and structural properties. These anomalies manifest themselves as an unusually strong temperature dependence in properties that are normally temperature-independent, particularly in the high-temperature superconductors such as V_3Si ($T_c = 17$ °K) and Nb_3Sn ($T_c = 18$ °K). As a result of their unique properties, these two compounds have been the most thoroughly studied members of this extensive family of fifty or more A_3B compounds. Recent review articles by Testardi[1] and Weger and Goldberg[2] summarize the current status of two decades of combined experimental and theoretical effort to measure, correlate, and interpret the normal- and superconducting-state properties of these and other closely related A15 compounds.

The present investigation is concerned with four particular A15 compounds, V_3Si, V_3Ge, Nb_3Al, and Nb_3Sn. These include two compounds whose properties are consistently anomalous (V_3Si and Nb_3Sn) and two where these anomalies are either absent entirely or present on a somewhat reduced scale (V_3Ge and Nb_3Al). Table I summarizes the presence or absence of these anomalies in the various physical properties within this group of A15 compounds. In regard to the structural transformation, Testardi[1] has emphasized that not all V_3Si

and Nb_3Sn samples undergo a cubic-to-tetragonal transformation at low temperatures. These differences among individual samples are generally attributed to deviations from perfect stoichiometry, though a recent model[3] emphasizes the importance of vacancies.

Two different mechanisms have been proposed to explain the origin of these anomalous properties. The first involves an unusually sharp peak in the electronic density of states near the Fermi energy, $N(E_F)$. The detailed shape of the $N(E)$ curve near E_F is not critical in these models, since qualitatively similar results are obtained by Clogston and Jaccarino[4] with a parabolic peak, Labbé and Friedel[5] with a square-root singularity, and Cohen et al.[6] with a simple step function. According to these models, $N(E_F)$ (per A atom) is typically 2–3 times larger than that derived by McMillan[7] for V and Nb metals from specific-heat and superconductivity data. More important, these models infer that $N(E)$ changes abruptly within a few meV to a small fraction of its value at E_F.

The second mechanism, which has been proposed by Testardi,[1,8] emphasizes the phonon rather than the electronic density of states. According to this model, the unusually large anharmonic motion of the atoms in the A15 lattice at low temperatures is responsible for significant corrections to the specific heat and produces a strong temperature-dependent phonon enhancement of the electronic properties of these materials. Testardi estimates that the usual methods for analyzing specific-heat data overestimate the electronic term γ by (10–20)%. This model suggests a somewhat smaller value for

TABLE I. Correlation between T_c and the occurrence of anomalies in the physical properties of the A15 compounds that are involved in the present study.

	V_3Si	V_3Ge	Nb_3Al	Nb_3Sn	References
T_c (°K)	17.1	6.1	18.6	18.0	a, a, b, c
Specific heat	yes	no	no	yes	d, d, b, d
Magnetic susceptibility	yes	yes	no	yes	e, e, b, f
Knight shift	yes	yes	no	yes	g, g, b, h
Resistivity	yes	yes	⋯	yes	i, i, ..., j
Elastic constants	yes	no	yes	yes	k, l, l, m
Structural transformation	yes	no	no	yes	n, o, b, p

[a]G. F. Hardy and J. K. Hulm, Phys. Rev. 93, 1004 (1954).
[b]Reference 46.
[c]B. T. Matthias et al., Phys. Rev. 95, 1435 (1954).
[d]Reference 44.
[e]H. J. Williams and R. C. Sherwood, Bull. Am. Phys. Soc. 5, 430 (1960).
[f]Reference 6.
[g]W. E. Blumberg et al., Phys. Rev. Lett. 5, 149 (1960).
[h]R. G. Shulman et al., Phys. Rev. Lett. 1, 278 (1958).
[i]M. P. Serachik et al., Can. J. Phys. 41, 1542 (1963).
[j]D. W. Woodard and G. D. Cody, RCA Rev. 25, 393 (1964).
[k]L. R. Testardi et al., Phys. Rev. Lett. 15, 250 (1965).
[l]L. R. Testardi et al., Phys. Rev. 154, 399 (1967).
[m]K. R. Keller and J. J. Hanak, Phys. Rev. 154, 628 (1967).
[n]B. W. Batterman and C. S. Barrett, Phys. Rev. Lett. 13, 390 (1964).
[o]B. W. Batterman (unpublished).
[p]R. Mailfert et al., Phys. Lett. A 24, 315 (1967).

the band $N(E_F)$ and a less abrupt variation with energy.

Most simplified band models for the A15 compounds emphasize the fact that the A atoms form three sets of mutually perpendicular chains for which the interatomic separation along a given chain is about 20% smaller than that between chains. Weger[9] suggested that this would result in a one-dimensional band structure and Fermi surface for these compounds, provided that the second-neighbor interchain interactions were negligible. This forms the basis for the Labbé-Friedel linear-chain model,[5] which treats the A-atom d bands as being purely one-dimensional in character. These d bands are overlapped by a broad s-p band such that E_F falls within a few meV of a square-root singularity in $N(E)$ for the $m_l = \pm 2$ d subband.

Previous augmented-plane-wave (APW) band-structure calculations for several A15 compounds (V_3Si, V_3Ga, V_3Ge, etc.) by the author[10] (hereafter referred to as I) revealed no evidence for the extremely flat A-atom d bands that this one-dimensional model implies. In fact, a careful analysis of these APW results in terms of a tight-binding model suggests that the effects of second-neighbor (interchain) d-d interactions on the band structure are comparable to those arising from nearest-neighbor (intrachain) interactions. Since these calculations were limited to energy-band states at symmetry points in the Brillouin zone, it was possible to calculate only a rather crude $N(E)$ curve for a typical compound, V_3Ga.

In order to extract more detailed information from these limited results, Weger, Goldberg, and co-workers[2] have applied the linear-combination-of-atomic-orbitals (LCAO) interpolation method[11] to fit the APW results in I. Their initial efforts involve a simplified approach that has been described as the coupled-chain model[2] or the independent-band approximation (IBA).[12] This IBA model includes both intrachain and interchain d-d interactions within a given d subband. However, it omits all hybridization interactions between the four different A-atom d subbands as well as many p-d interactions between the B-atom p and the A-atom d orbitals. As a result of these approximations, the IBA model produces extremely large peaks in $N(E)$, resulting from bands that are perfectly flat throughout the ΓXM plane of the Brillouin zone.

Recently, Goldberg[12] has removed many of the simplifying approximations of the IBA model in his coupled-band approximation (CBA), which is essentially equivalent to the standard Slater-Koster LCAO interpolation method.[11] Although Goldberg
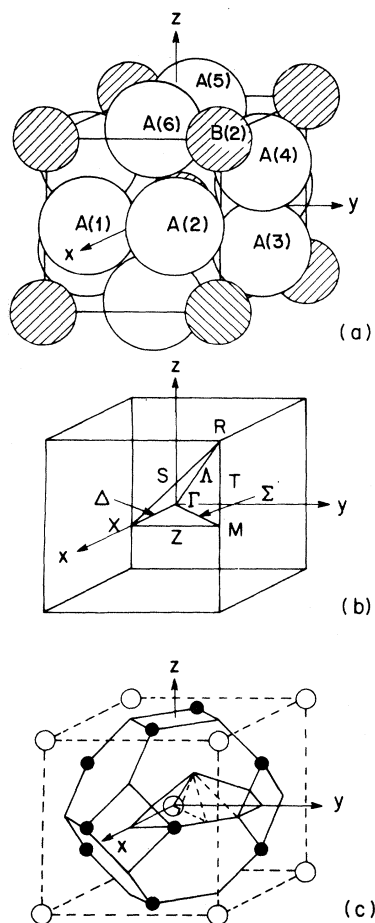
FIG. 1. (a) Primitive unit cell for A15 compounds. (b) Brillouin zone for the simple-cubic Bravais lattice. (c) Symmetry of the irreducible wedge representing $\frac{1}{48}$ of the unit cell.

claims that the CBA results justify the validity of the IBA model, it is clear from his $N(E)$ curves for V_3Ga that interband hybridization washes out the sharpest peaks in the IBA results. Neither model predicts a peak in $N(E)$ near E_F for the high-T_c compounds unless substantial adjustments to the LCAO parameters are introduced. Neither model provides an accurate fit to the APW energy-band results of I near E_F.

The purpose of the present investigation is to provide a more accurate band-structure model for several A15 compounds, including V_3Si, V_3Ge, Nb_3Al, and Nb_3Sn. This study involves the application of the standard Slater-Koster LCAO interpolation method[11] to fit the results of a new series of APW calculations for these compounds. The present LCAO model is analogous to the one that has been applied previously to several transition-metal oxides with the ReO_3,[13] rock-salt,[14] and perovskite[15] structures. It differs from Goldberg's

CBA model in two respects. First, it includes covalency interactions between the B-atom s and A-atom d orbitals. Second, it treats overlap effects between the B-atom s-p and the A-atom d orbitals explicitly in terms of a nondiagonal overlap matrix.[13-15]

Some effort has been made to improve the overall accuracy of the present APW results relative to those of the previous calculations in I. For example, the present APW calculations include corrections to the muffin-tin potential in the region between the APW spheres. In addition, the number of APW basis functions has been increased in order to reduce convergence errors from about 0.03 Ry in I to 0.003 Ry in the present study.

Details of the present APW and LCAO calculations for the A15 structure are summarized in Sec. II. The results of these combined APW-LCAO calculations are presented in Sec. III, including $E(\vec{k})$ and $N(E)$ curves. The present APW-LCAO results are then applied in Sec. IV to evaluate the accuracy of the simplified band models that have been applied to describe the electronic structure of these A15 compounds. Finally, in Sec. V, we discuss the accuracy of the present APW-LCAO band model in terms of the available experimental data.

II. DETAILS OF THE CALCULATION

A. A15 structure

The primitive unit cell for A_3B compounds with the A15 structure is shown in Fig. 1(a). Each cubic cell contains two A_3B molecules or a total of eight atoms. The two B atoms, $B(1)$ and $B(2)$, occupy the body-centered cubic positions $a(0, 0, 0)$ and $a(\frac{1}{2}, \frac{1}{2}, \frac{1}{2})$, while the six A atoms $[A(1)-A(6)]$ are located on the cube faces at the positions $a(\frac{1}{2}, \pm\frac{1}{4}, 0)$, $a(0, \frac{1}{2}, \pm\frac{1}{4})$, and $a(\pm\frac{1}{4}, 0, \frac{1}{2})$, where a is the cubic lattice constant. The A atoms form three sets of orthogonal chains along the $y[A(1), A(2)]$, $z[A(3), A(4)]$, and $x[A(5), A(6)]$ axes, respectively. The Brillouin zone for the simple-cubic Bravais lattice is shown in Fig. 1(b), where the standard labels are used to identify symmetry points and lines.

The space group for the cubic A15 structure is O_h^3, which is a nonsymmorphic space group. With the origin at a B-atom site, the symmetry operations for this space group are of two types. First, there are 24 space-group operations of the form $\{\alpha|\vec{R}_n\}$, where α is a point-group operation in T_h and $\vec{R}_n$ is a primitive translation $\vec{R}_n = a(n_1\hat{i} + n_2\hat{j} + n_3\hat{k})$. Here, the n_i are integers, and $\hat{i}$, $\hat{j}$, and $\hat{k}$ are unit vectors along the x, y, and z axes, respectively. In addition, there are 24 space-group operations $\{\alpha'|\vec{R}_n + \vec{\tau}\}$, where α' spans the remaining 24 point-group operations in O_h and $\vec{\tau}$ is a non-

TABLE II. Angular symmetry of atomiclike orbitals $\varphi_{l\alpha}(\vec{r} - \vec{r}_n) \equiv \alpha_n$ which transform irreducibly under the point group D_{2d} at A-atom sites along the y, z, and x axes, where $\vec{r}_{1/2} = a(\frac{1}{2}, \mp\frac{1}{4}, 0)$, $\vec{r}_{3/4} = a(0, \frac{1}{2}, \mp\frac{1}{4})$, and $\vec{r}_{5/6} = a(\mp\frac{1}{4}, 0, \frac{1}{2})$, respectively.

l	WG[a] (BSW[b])	$n=1/2$	$n=3/4$	$n=5/6$
s	$\sigma(W_1)$	s_n	s_n	s_n
p	$\pi(W_3)$	z_n, x_n	x_n, y_n	y_n, z_n
p	$\delta_1(W_2)$	y_n	z_n	x_n
d	$\sigma(W_1)$	$(3y^2 - r^2)_n$	$(3z^2 - r^2)_n$	$(3x^2 - r^2)_n$
d	$\pi(W_3)$	zy_n, xy_n	xz_n, yz_n	xy_n, zx_n
d	$\delta_1(W_2)$	$(z^2 - x^2)_n$	$(x^2 - y^2)_n$	$(y^2 - z^2)_n$
d	$\delta_2(W_1')$	zx_n	xy_n	yz_n

[a]Notation of Weger and Goldberg, Ref. 2.
[b]Notation of Bouckaert, Smoluchowski, and Wigner, Ref. 18.

primitive translation, $\vec{\tau} = \frac{1}{2} a(\hat{i} + \hat{j} + \hat{k})$. The irreducible representations for the O_h^3 space group are available in the literature.[16,17] The present notation is identical with that used in I.

In working out the detailed form of the LCAO matrix for the $A15$ structure, it is convenient to utilize atomiclike functions which transform irreducibly under the point groups at the A-atom (D_{2d}) and B-atom (T_h) sites. The s and p orbitals at a B-atom site satisfy this condition. The proper choice of basis functions at the A-atom sites is indicated in Table II. The irreducible representations for D_{2d} are identified using the notation of Weger and Goldberg[2] (WG) and Bouckaert et al.[18] (BSW). The A-atom p and d levels (or bands) are subdivided into two (π, δ_1) and four (σ, π, δ_1, δ_2) components, respectively. These are analogous to the more familiar separation of a d band or level into its e_g and t_{2g} components in an octahedral environment. We represent the s, p, and d orbitals at an A-atom site by $\varphi_{l\alpha}(\vec{r} - \vec{r}_n) \equiv \alpha_n$ such that an orbital at site $A(3)[A(4)]$ is denoted by $\alpha_3(\alpha_4)$,

where $\alpha = s$, x, y, z, xy, yz, zx, $3z^2 - r^2$, or $x^2 - y^2$. The corresponding orbitals at the remaining sites are obtained by cyclically permuting (x, y, z).

For a given wave vector $\vec{k}$, linear combinations of the Bloch sums formed from these orbitals transform irreducibly under the O_h^3 space-group operations. These results are summarized in Table III for wave vectors $\vec{k}$ at Γ, X, M, and R both for the A-atom s-p-d and the B-atom s-p orbitals. The appropriate space-group representation is identified by its subscript, so that, for example, the entries 1, 12, 25 under Γ denote the irreducible representations Γ_1, Γ_{12}, and Γ_{25}, respectively. Repeated entries indicate that the same representation occurs more than once.

Both V_3Si and Nb_3Sn are known to undergo cubic-to-tetragonal structural transformations at low temperatures.[19,20] The crystal structure in the tetragonal phase has been identified only in the case of Nb_3Sn. Shirane and Axe[21] find that the Nb_3Sn space group reduces from O_h^3 in the cubic phase to D_{4h}^9 in the tetragonal phase at temperatures below 43 °K. The number of atoms in the primitive unit cell is unchanged as a result of this tetragonal distortion. Lattice-parameter measurements show that this distortion is opposite in Nb_3Sn and V_3Si, where $c/a = 0.9938$ and 1.0024, respectively.

A knowledge of the low-temperature space group enables one to determine the manner in which the cubic energy-band states are split in the tetragonal phase. These results are summarized in Table IV for D_{4h}^9. Here, the tetragonal c axis is identified with the z direction, and wave vectors $\vec{k}$ are expressed in units $(k_x a/\pi, k_y a/\pi, k_z c/\pi)$. In the tetragonal phase, $M(\pm 1, \pm 1, 0)$ is no longer equivalent to $M(\pm 1, 0, \pm 1)$ or $M(0, \pm 1, \pm 1)$, and $X(0, 0, \pm 1)$ is distinct from both $X(\pm 1, 0, 0)$ and $X(0, \pm 1, 0)$. For the D_{4h}^9 space group, the group of the wave vector is unchanged for $M(\pm 1, \pm 1, 0)$ and $X(0, 0, \pm 1)$, so that no new splittings occur at these points. However, degeneracies are reduced at $\Gamma(0, 0, 0)$,

TABLE III. Space-group symmetry of Bloch sums formed from A-atom s, p, and d orbitals and B-atom s-p orbitals for the $A15$ structure at Γ, X, M, and R.

Atom	Orbital	Γ	X	M	R
A	$s(\sigma)$	1,12,25	1,1,3	1,4,5,6,9	4
	$p(\pi)$	15,25,15',25'	1,2,3,4,4,4	2,3,6,7,9,9,10,10	1,2,3,4
	$p(\delta_1)$	2,12,15	1,1,3	1,2,5,8,9	4
	$d(\sigma)$	1,12,25	1,1,3	1,4,5,6,9	4
	$d(\pi)$	15,25,15',25'	1,2,3,4,4,4	2,3,6,7,9,9,10,10	1,2,3,4
	$d(\delta_1)$	2,12,15	1,1,3	1,2,5,8,9	4
	$d(\delta_2)$	1',12',25'	2,2,3	3,4,5,8,10	4
B	s	1,2	1	9	3
	p	15,25	1,3,4	1,2,5,6,10	4

TABLE IV. Effect of a tetragonal distortion (D_{4h}^9) on cubic (O_h^3) energy-band states.

O_h^3	D_{4h}^9	O_h^3	D_{4h}^9	O_h^3	D_{4h}^9
	$\Gamma(0,0,0)$		$M(1,1,0)$		$M(1,0,1)$
Γ_1	Γ_1^{*a}	M_1	M_1	M_1	M_3^{*b}
Γ_2	Γ_2^*	M_2	M_2	M_2	M_1^*
Γ_{12}	$\Gamma_1^*+\Gamma_2^*$	M_3	M_3	M_3	M_2^*
Γ_{15}	$\Gamma_4^*+\Gamma_5^*$	M_4	M_4	M_4	M_1^*
Γ_{25}	$\Gamma_3^*+\Gamma_5^*$	M_5	M_5	M_5	M_3^*
$\Gamma_{1'}$	Γ_2^*	M_6	M_6	M_6	M_1^*
$\Gamma_{2'}$	$\Gamma_{1'}^*$	M_7	M_7	M_7	M_2^*
$\Gamma_{12'}$	$\Gamma_{1'}^*+\Gamma_{2'}^*$	M_8	M_8	M_8	M_4^*
$\Gamma_{15'}$	$\Gamma_4^*+\Gamma_5^*$	M_9	M_9	M_9	$M_1^*+M_3^*$
$\Gamma_{25'}$	$\Gamma_3^*+\Gamma_5^*$	M_{10}	M_{10}	M_{10}	$M_2^*+M_4^*$
	$X(0,0,1)$		$X(1,0,0)$		$R(1,1,1)$
X_1	X_1	X_1	$X_1^*+X_3^{*b}$	$R_1-R_2^{c}$	$R_1^*+R_1^{*d}$
X_2	X_2	X_2	$X_4^*+X_2^*$	R_3	R_1^*
X_3	X_3	X_3	$X_3^*+X_4^*$	R_4	$R_2^*+R_3^*+R_4^*$
X_4	X_4	X_4	$X_2^*+X_1^*$		

[a]The representations Γ_i^* are equivalent to M_i in Table V of BSW (Ref. 18).

[b]The representations X_i^* and M_i^* correspond to N_i in Table XII of BSW (Ref. 18), with $C_4^2 = C_{2x}$, $C_{2\|}$, and $C_{2\perp} = C_{2z}$.

[c]R_1 and R_2 are time-reversal degenerate.

[d]$R_1^*-R_4^*$ are four two-dimensional representations.

$M(\pm 1, 0, \pm 1) = M(0, \pm 1, \pm 1)$, $X(\pm 1, 0, 0) = X(0, \pm 1, 0)$, and $R(\pm 1, \pm 1, \pm 1)$, where the groups of the wave vector are D_{4h}, D_{2h}, D_{2h}, and D_{4h}, respectively.

B. APW calculations

The procedures and techniques that are involved in the present APW calculations are similar to those described in I. However, two modifications have been introduced in order to improve the overall accuracy of the present results. First, the APW calculations now include a sufficient number of basis functions to reduce convergence errors from 0.03 Ry in I (particularly at the X, M, and R points) to about 0.003 Ry in the present study. Second, the present calculations involve a crystal potential that is no longer required to be constant in the regions between the APW spheres.

The lattice parameters and APW sphere radii for the A_3B compounds included in the present study are listed in Table V. The A-atom sphere radii are assigned their maximum value, $R_A = a/4$, such that neighboring spheres touch along the axes of the chains. This optimizes the convergence of the APW method.[22] The B-atom sphere radii are less critical since they represent nontransition elements, for which the convergence is more rapid. These radii are arbitrarily assigned values that are about 14% smaller than their maximum value,

TABLE V. Lattice parameters and APW sphere radii for the $A15$ compounds included in the present study.

A_3B	a (Å)	R_A (a. u.)	R_B (a. u.)
V$_3$Si	4.722	2.2307	2.4630
V$_3$Ge	4.769	2.2756	2.5123
Nb$_3$Al	5.187	2.4505	2.7054
Nb$_3$Sn	5.282	2.4954	2.7549

$R_B(\text{max}) = (\sqrt{5} - 1)R_A$. This choice, which is similar to that in I, minimizes the nonspherical corrections to the potential within the B-atom spheres.

As in the earlier calculations, the crystal potentials for each compound are derived from a superposition of Hartree-Fock-Slater atomic charge densities.[23] The assumed atomic configuration for the A atoms (V or Nb) is d^4s, while that of the B atoms is either s^2p (Al) or s^2p^2 (Si, Ge, or Sn). The methods that are applied to calculate the muffin-tin potential $V_m(\vec{r})$ plus the Fourier coefficients $V_A(\vec{K}_j)$ of the corrections to the muffin-tin potential in the region between the APW spheres are analogous to those described earlier.[13-15] In the $A15$ structure, the latter calculation involves integrals over $\frac{1}{48}$ of the unit cell shown in Fig. 1(c). In the region between the spheres, it is found that the peak-to-peak variations of the potential from the muffin-tin constant are in the range 0.70–0.85 Ry. The Fourier coefficients of these corrections, $V_A(\vec{K}_j)$, are relatively small. Their magnitude is comparable with that found in the rock-salt[14] and perovskite[15] structures. The calculated values for the lowest-order nonvanishing coefficients are listed in Table VI along with the muffin-tin constant, V_{m0}.

The present calculations neglect the nonspherical corrections to the muffin-tin potential inside the APW spheres. These corrections are largest within a spherical shell in the neighborhood of the sphere radii. A detailed examination shows that these corrections are relatively small within the B-atom spheres, where the variation in the potential along different directions is typically 0.2

TABLE VI. Values for the muffin-tin constants V_{m0} and the nine lowest-order nonvanishing Fourier coefficients $V_A(\vec{K}_j)$ (Ry).

$\vec{K}_j(a/2\pi)$	V$_3$Si	V$_3$Si[a]	V$_3$Ge	Nb$_3$Al	Nb$_3$Sn
V_{m0}	−1.3889	−1.4541	−1.3550	−1.2973	−1.2725
(1,1,0)	−0.0004	0.0029	−0.0007	0.0025	0.0002
(2,0,0)	−0.0110	−0.0187	−0.0101	−0.0130	−0.0118
(2,1,0)	0.0022	0.0049	0.0021	0.0007	0.0002
(2,1,1)	0.0042	0.0046	0.0041	0.0025	0.0041
(2,2,0)	0.0024	0.0007	0.0025	0.0009	0.0021
(2,2,2)	−0.0067	−0.0113	−0.0065	−0.0069	−0.0074
(3,1,0)	−0.0009	−0.0027	−0.0007	−0.0018	−0.0012
(3,2,0)	0.0029	0.0078	0.0027	0.0034	0.0033
(3,2,1)	0.0012	0.0035	0.0010	0.0022	0.0016

[a]Vanadium APW sphere radius reduced by 10%.

Ry. By comparison, the corresponding variations within the A-atom spheres are generally twice as large.

In order to estimate the effect of these non-spherical corrections on the present energy-band results, we have performed limited APW calculations for V_3Si in which the vanadium sphere radius is reduced by 10% from its maximum value, $R_V = a/4$. This transfers the bulk of the nonspherical corrections to regions outside the APW spheres, where they are treated exactly in APW formalism by means of the Fourier coefficients $V_A(\vec{K}_j)$. The disadvantage of this procedure is that it adversely affects the convergence of the APW method such that an additional 100 basis functions are required in order to achieve the same degree of convergence.[22] By comparing the results of fully converged APW calculations for V_3Si with $R_V = a/4$ and $R'_V = 0.9 R_V$, we estimate that these nonspherical corrections will alter the energy eigenvalues by less than 0.01 Ry. The average shift is about 0.003 Ry. The Fourier coefficients for this latter calculation are also included in Table VI.

Approximately 400 APW basis functions are required in order to reduce convergence errors to about 0.003 Ry in the $A15$ compounds with R_A at its maximum value. This precludes the possibility of performing unsymmetrized calculations for these materials or calculating $E(\vec{k})$ at general points in the Brillouin zone. It even discourages calculations along symmetry lines, where the dimension of the symmetry-reduced APW matrix generally exceeds 100×100. Even at the high symmetry points such as Γ, X, M, and R, the maximum dimension of the symmetrized APW matrix is 65×65.

The present APW programs also exploit the fact that the logarithmic derivatives $u'_l(R, E)/u_l(R, E)$ are, to a good approximation, linear functions of the energy E for $l \geq 4$. This greatly reduces the size of the computer core that is required in APW calculations and improves the overall efficiency of the programs with little sacrifice in accuracy.

C. LCAO model

A careful study of the APW results for V_3Ga in Fig. 4 of I suggests that the combined interpolation scheme[24] is probably the optimum method for interpolating the lowest valence and conduction bands in the $A15$ compounds. This is perhaps not unexpected since each of the constituents can be treated by either the combined interpolation (V or Nb) or pseudopotential methods (Si, Ge, Al, or Sn). The main drawback to this approach is the large number of pseudo-plane-wave states that are required. In contrast to the fcc structure[24] where the plane-wave block is 4×4, it seems likely that the $A15$ structure will require a minimum of

24 plane-wave states. These, combined with the 30 A-atom d states, will yield a model Hamiltonian matrix with minimum dimensions 54×54.

The main advantage of the combined-interpolation method over the standard LCAO approach is that it usually requires about half as many parameters to achieve the same degree of accuracy. On the other hand, the LCAO method readily provides energy-band results that reflect the full symmetry of the crystal. It is necessary to introduce the somewhat artificial symmetrizing factors[24] within the plane-wave and hybridization blocks to recover this symmetry within the framework of the combined-interpolation scheme. This problem is particularly important in compounds with non-symmorphic space groups where highly-degenerate bands are common for wave vectors on the surface of the Brillouin zone. The point R is an important example of this phenomena in the O_h^3 space group, since each state is either sixfold (R_4), fourfold $(R_1 - R_2)$, or twofold (R_3) degenerate.

After careful consideration of these alternatives, it was decided to apply the standard LCAO interpolation method to the $A15$ compounds. In the present application, this LCAO model involves a total of 38 basis functions of the form

$$b_n^i(\vec{k}) = N^{-1/2} \sum_j e^{i\vec{k} \cdot (\vec{R}_j - \vec{r}_i)} \varphi_n(\vec{r} - \vec{R}_j - \vec{r}_i) , \quad (1)$$

where φ_n represents an atomic orbital with quantum numbers n at site $\vec{r}_i$ in the unit cell. These Bloch sums are formed from 30 A-atom d orbitals and 8 B-atom s-p orbitals. The A-atom s-p orbitals are omitted; their inclusion would increase the dimension of the LCAO matrix from 38×38 to 62×62 and significantly increase the number of LCAO parameters.

The tedious task of working out the detailed expressions for the 741 independent matrix elements of this 38×38 model Hamiltonian is simplified if the A-atom d orbitals φ_d transform irreducibly under the D_{2d} point group. In that case, one can generate the entire 30×30 d submatrix $H_{d,d}$ from two 10×10 submatrices $\underline{A}(\xi, \eta, \zeta)$ and $\underline{B}(\xi, \eta, \zeta)$ by cyclic permutation of $(\xi, \eta, \zeta) \equiv (k_x a, k_y a, k_z a)$. If we denote the 10×10 matrix that describes the "intrachain" $d - d$ interactions between $b_d^3(\vec{k})$ and $b_d^4(\vec{k})$ by $\underline{A}(\xi, \eta, \zeta)$ and the "interchain" $d - d$ interactions between $b_d^3(\vec{k})$, $b_d^4(\vec{k})$ and $b_d^5(\vec{k})$, $b_d^6(\vec{k})$ by $\underline{B}(\xi, \eta, \zeta)$, then

$$\underline{H}_{d,d} = \begin{pmatrix} \underline{A}(\zeta, \xi, \eta) & \underline{B}(\zeta, \xi, \eta) & \underline{B}(\eta, \zeta, \xi)^\dagger \\ \underline{B}(\zeta, \xi, \eta)^\dagger & \underline{A}(\xi, \eta, \zeta) & \underline{B}(\xi, \eta, \zeta) \\ \underline{B}(\eta, \zeta, \xi) & \underline{B}(\xi, \eta, \zeta)^\dagger & \underline{A}(\eta, \zeta, \xi) \end{pmatrix} . \quad (2)$$

Similar simplifications also occur in the 2×30 s-d submatrix $\underline{H}_{s,d}$ and the 6×30 p-d submatrix $\underline{H}_{p,d}$.

The entire LCAO energy matrix $\underline{H}$ (as well as

the overlap matrix $\underline{S}$) can be made real by a unitary transformation. Within $\underline{H}_{d,d}$, this involves linear combinations of "intrachain" Bloch sums of the type $(b_{xy}^3 + b_{xy}^4)/\sqrt{2}$ and $i(b_{xy}^3 - b_{xy}^4)/\sqrt{2}$, etc. Similarly, the $\underline{H}_{s,p}$ and $\underline{H}_{p,d}$ submatrices are real if the Bloch sums for the B-atom p orbitals b_x^1, b_y^1, ..., b_z^2 are replaced by ib_x^1, ib_y^1, ..., ib_z^2.

Even with these simplifications, the LCAO matrix $\underline{H}$ remains rather complicated. For example, each of the 100 matrix elements in the 10×10 submatrix $\underline{B}$ of Eq. (2) is nonvanishing. These matrix elements involve the appropriate energy integral $E_{\alpha,\beta}(\vec{r}_i - \vec{r}_j)$ times a product involving ± 4 ($\sin\alpha$ or $\cos\alpha$)$\times$($\sin\beta$ or $\cos\beta$)$\times$($\sin\gamma$ or $\cos\gamma$), where $(\alpha, \beta, \gamma) = (\frac{1}{4}\xi, \frac{1}{2}\eta, \frac{1}{4}\zeta)$ for nearest-neighbor interchain interactions. Second-neighbor interchain d-d interactions involve a sum of two such terms with $(\alpha, \beta, \gamma) = (\frac{1}{4}\xi, \frac{1}{2}\eta, \frac{3}{4}\zeta)$ and $(\frac{3}{4}\xi, \frac{1}{2}\eta, \frac{1}{4}\zeta)$, respectively.

Briefly, we consider the simplifying assumptions that successively reduce this 38×38 LCAO matrix to the Weger-Goldberg IBA model and finally the Labbé-Friedel linear-chain model. In their IBA model, Weger and Goldberg neglect off-diagonal interband matrix elements in $\underline{A}$ and $\underline{B}$ of Eq. (2) between σ, π, δ_1, and δ_2 states. This is an approximation since, even at symmetry points (see Table III), nonvanishing off-diagonal matrix elements are expected between states that transform according to the same representation. The neglect of these interband matrix elements reduces the 30×30 matrix $\underline{H}_{d,d}$ to three noninteracting 6×6 submatrices (σ, δ_1, and δ_2) and one 12×12 submatrix (π).

The IBA model also simplifies the s-d and p-d interactions. It sets $\underline{H}_{s,d} = 0$ and restricts p-d interactions to those between p and δ_1-type states. The net result is to reduce the full 38×38 LCAO matrix into five noninteracting submatrices that include one of order 2 (B-atom s states), two of order 6 (A-atom σ and δ_2 states), and two of order 12 (π and p-δ_1 states). We shall examine the validity and consequences of these approximations in Sec. IV B.

The linear-chain model of Labbé and Friedel sets $\underline{H}_{s,d} = \underline{H}_{p,d} = \underline{B} = 0$, and assumes that the submatrix $\underline{A}$ in Eq. (2) is diagonal. These diagonal matrix elements are given by Eq. (2) in I. As shown in Sec. IV A, these simplications produce a band structure with a large number of accidental degeneracies at symmetry points and along symmetry lines in the Brillouin zone. They produce bands which are perfectly flat everywhere in the $\Gamma X M$ plane. These flat bands are the source of the square-root singularities in $N(E)$ for the linear-chain model. While the IBA model removes many of these accidental degeneracies, this approximation does yield a band (δ_2) that is perfectly flat

everywhere in the $\Gamma X M$ plane, thereby producing a sharp peak in $N(E)$.

D. Determination of LCAO parameters

In order to fit the APW results at Γ, X, M, and R, one must reduce the full 38×38 LCAO matrix into its noninteracting submatrices $\underline{H}^\alpha$ for these wave vectors. According to Table III, this yields five submatrices $\underline{H}^\alpha$ of order one (Γ_1', Γ_{12}', Γ_{15}', M_7, $R_1 - R_2$), eight of order two (Γ_1, Γ_2, Γ_{12}, Γ_{25}, M_3, M_4, M_8, R_3), six of order three (Γ_{15}, Γ_{25}, X_2, M_1, M_2, M_6), three of order four (X_4, M_5, M_{10}), three of order five (X_3, M_9, R_4), and one of order seven (X_1). (We treat the time-reversal degenerate states[16] $R_1 - R_2$ as a single four-fold degenerate level.) Weighting each eigenvalue equally, regardless of its degeneracy, this yields a total of 73 APW energies which are to be fit by this LCAO model.

The problem of determining optimum values for the LCAO parameters requires a nonlinear-least-squares fitting technique, since it is only in those cases where H^α is of order one that the energy is a linear function of these parameters. In all other cases, the LCAO eigenvalues are nonlinear functions of the parameters. The methods that have been applied to determine the present $A15$ LCAO parameters are analogous to those described earlier in a similar study involving compounds with the rock-salt structure.[14]

Of course, the $A15$ structure is much more complicated than that of rock salt, and this leads to a large number of independent Slater-Koster LCAO energy integrals, $E_{\alpha,\beta}(\vec{r}_i - \vec{r}_j)$. If each of these is varied independently, this can lead to spurious minima in the nonlinear least-squares fitting procedure such that the final set of parameters is dependent on the assumed starting values. To eliminate this difficulty, we have determined the present LCAO parameters in two stages. In the first stage, we apply a very simplified two-center model to fit the APW results in terms of 21 independent parameters. This two-center model includes first- and second-neighbor B-atom s-s, p-p, and A-atom d-d interactions plus nearest-neighbor overlap and covalency effects between the A-atom d and the B-atom s-p orbitals. With these approximations, the above nonlinear least-squares procedure leads to the unique two-center parameters that are listed in Table VII within ten interations.

These parameters are then used as starting values for the final stage, where the two-center approximation is partially relaxed and twelve states near E_F are weighted more heavily in the fitting procedure. At this stage, first- and second-neighbor d-d interactions are treated in terms of the energy integrals $E_{\alpha,\beta}(\vec{r}_i - \vec{r}_j)$ rather than in the two-center approximation, while third- and fourth-neighbor

TABLE VII. APW–LCAO two–center parameters (Ry) for V_3Si, V_3Ge, Nb_3Al, and Nb_3Sn.

Parameter	V_3Si	V_3Ge	Nb_3Al	Nb_3Sn
E_s	−0.7217	−0.7676	−0.4390	−0.5707
$(ss\sigma)_1$	−0.0084	−0.0075	−0.0075	−0.0062
$(ss\sigma)_2$	−0.0047	−0.0041	−0.0065	−0.0048
E_p	−0.2076	−0.2154	−0.0503	−0.1265
$(pp\sigma)_1$	0.0247	0.0265	0.0265	0.0212
$(pp\pi)_1$	−0.0144	−0.0137	−0.0098	−0.0092
$(pp\sigma)_2$	0.0256	0.0265	0.0178	0.0212
$(pp\pi)_2$	0.0016	0.0007	−0.0028	−0.0030
E_d	0.0265	0.0286	0.0549	0.0482
$(dd\sigma)_1$	−0.0730	−0.0719	−0.1025	−0.0963
$(dd\pi)_1$	0.0938	0.0897	0.0950	0.0941
$(dd\delta)_1$	−0.0325	−0.0303	−0.0286	−0.0272
$(dd\sigma)_2$	−0.0537	−0.0518	−0.0700	−0.0665
$(dd\pi)_2$	0.0391	0.0366	0.0351	0.0335
$(dd\delta)_2$	−0.0087	−0.0077	−0.0091	−0.0083
$(sd\sigma)$	−0.0840	−0.0856	−0.0574	−0.0743
S_s	0.1362	0.1237	0.1585	0.1235
$(pd\sigma)$	−0.0777	−0.0767	−0.0543	−0.0681
S_σ	0.1828	0.1832	0.2098	0.2053
$(pd\pi)$	0.0629	0.0607	0.0596	0.0578
S_π	−0.0250	−0.0314	−0.0417	−0.0373
rms error	0.022	0.020	0.023	0.020
Maximum error	0.062	0.054	0.065	0.056
Δ	−0.793	−0.769	−0.666	−0.652

d-d interactions are added in the two-center approximation. These represent a total of $5 + 13 + 3 + 3 = 24$ parameters, or a net increase of 18.[25] With these 39 LCAO parameters, the rms error is reduced to the range 0.014–0.018 Ry. If each state is weighted equally, the rms error is further reduced to 0.013–0.015 Ry.

One complicating feature of the APW results for the $A15$ compounds is the overlap of the lower portions of the A-atom s-p and d bands at $\Gamma(\Gamma_1, \Gamma_{12})$, $X(X_1)$, and $M(M_3, M_9)$ (see Figs. 4 and 5 of I). This difficulty is not present in the analogous, results for transition-metal oxides,[13-15] where the metal s-p bands are raised well above the d bands by strong covalency interactions with the oxygen s-p orbitals. As Goldberg[12] points out, these interactions are less effective in the $A15$ compounds where the A atoms outnumber the B's by a 3 to 1 ratio.

The main effect of this band overlap is to introduce some ambiguity in distinguishing between these A-atom s-p and d levels. This identification is important since, in the present LCAO model, the eigenvalues for the former levels are neglected while those for the latter are utilized in the nonlinear-least-squares fitting procedure. It is believed that the combined interpolation scheme would be particularly effective in resolving these ambiguities. After some experimentation, it was found that the most accurate LCAO fit is obtained if, among the ambiguous states (Γ_1, Γ_{12}, X_1, M_3, and M_9), those with lowest energy are assigned to the B-atom s-p and A-atom d bands. In addition to improving the

accuracy of the LCAO fit, this assumption has the important feature that all bands near and below the Fermi level are described by the LCAO model. This allows one to determine the Fermi energy entirely within the framework of this LCAO model.

This identification of levels differs from that of Weger and Goldberg in the[2] IBA and[12] CBA models. Their identification assigns two levels below E_F (Γ_{12} and X_1) to the A-atom s bands. Consequently, they are unable to calculate the Fermi energy directly from their IBA or CBA results. As discussed in Sec. IV B, the present 21 two-center parameter LCAO model has been applied to fit both the present and the IBA-CBA assignment of APW levels in V_3Ga. The former assignment yields an rms error of 0.021 Ry and a maximum error of 0.06 Ry; these errors increase to 0.031 Ry and 0.12 Ry, respectively, with the IBA-CBA assignment of APW levels.

For convenience in comparing $E(\vec{k})$ and $N(E)$ curves for different compounds in the following sections, the reference energies for the LCAO parameters in Table VII have been shifted relative to the muffin-tin constants V_{m0} in Table VI by an amount Δ. This corresponds to setting $E(\Gamma_{12}) = 0$ for the Γ_{12} state just below $E_F \approx 0.1$ Ry for V_3Ga in I. This shift is such that both the d-orbital energy E_d and the Fermi energy E_F are approximately zero in each compound.

III. APW-LCAO RESULTS

The present APW-LCAO energy-band results for V_3Si, V_3Ge, Nb_3Al, and Nb_3Sn are shown in Figs. 2–5. These $E(\vec{k})$ curves are derived from the 39-parameter LCAO fit (weighted near E_F) to 73 APW energy levels at symmetry points in the Brillouin zone that is described in Sec. II D. These
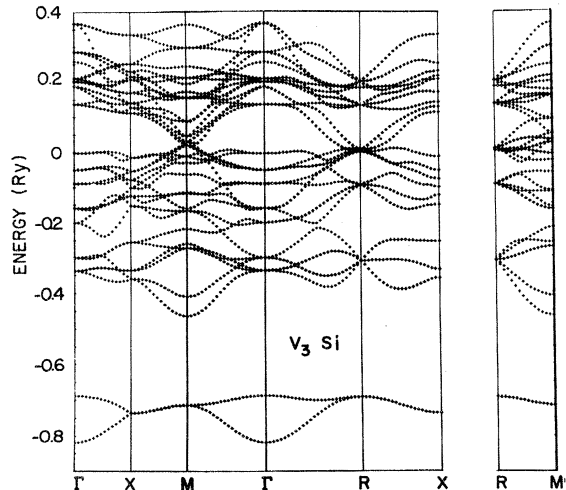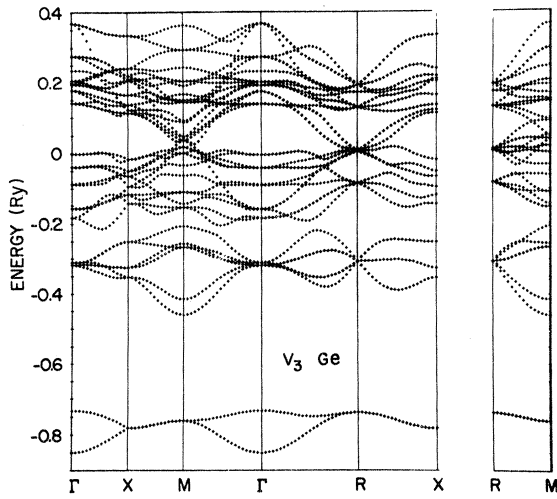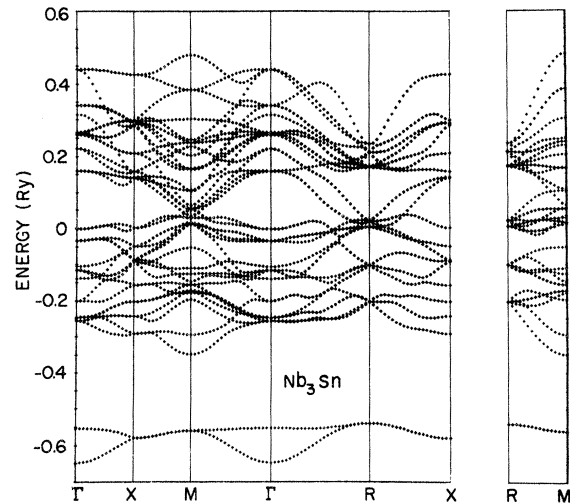

FIG. 2. APW–LCAO energy bands for V_3Si.

FIG. 3. APW-LCAO energy bands for V_3Ge.

FIG. 5. APW-LCAO energy bands for Nb_3Sn.

APW-LCAO results include all the bands shown in Fig. 4 of I for V_3Ga except for those that are identified as A-atom s-p states (the highest-energy states with Γ_1, Γ_{12}, X_1, M_3, and M_9 symmetry in Fig. 4 of I).[26]

Neglecting for the moment the effects of covalent mixing between the A-atom d and the B-atom s-p states, we can identify the lowest pair of bands as B-atom s states, the next six bands as B-atom p states, and the upper complex of thirty bands as A-atom d states. (Bands are most easily counted along the RX line, where each is doubly degenerate.[16,17]) In each compound, the Fermi energy falls slightly above the zero of energy. Each unit cell contains either 36 (Nb_3Al) or 38 (V_3Si, V_3Ge, Nb_3Sn) valence and conduction electrons, so that the Fermi level occurs in the vicinity of the 18th or

19th band, assuming each is doubly occupied. In each compound, there is a total of 20 bands below E_F at the Γ and X points and 14–18 bands at the M and R points of the Brillouin zone.

This sharp distinction between the A-atom d and the B-atom s-p bands is blurred by the effects of covalent bonding, particularly that between the A-atom d and B-atom p orbitals, for which the energy separation is smaller. As a result of p-d bond formation, the LCAO p charge density in V_3Si, for example, occurs not only in the energy range of the occupied bands (bonding states between -0.20 and -0.45 Ry in Fig. 2), but also among the unoccupied bands (antibonding states between 0.15 and 0.35 Ry), with lesser amounts at intermediate energies.

In comparing the results of Figs. 2–5, it is clear that the main difference between the band structures for the various A_3B compounds is in the position of the B-atom s-p bands relative to the A-atom d bands. These trends are reflected in the two-center LCAO parameters of Table VII, where $E_d - E_s$ and $E_d - E_p$ are largest for V_3Si and V_3Ge, intermediate for Nb_3Sn, and smallest for Nb_3Al. In Figs. 2–5, the d-band width tends to be slightly greater in the Nb (0.7 Ry) than in the V (0.6 Ry) compounds, which is a typical feature of calculations for transition metals and transition-metal compounds involving $4d$ and $3d$ elements.

A more detailed plot of these APW-LCAO bands in the vicinity of E_F is shown in Fig. 6. The twelve states near E_F that were weighted in the LCAO fit are enclosed in parentheses in Fig. 6(a). The Fermi level for each compound is indicated by a dashed horizontal line. The results of Fig. 6 indicate a possible limitation of the present APW-LCAO model. In particular, it is not clear whether
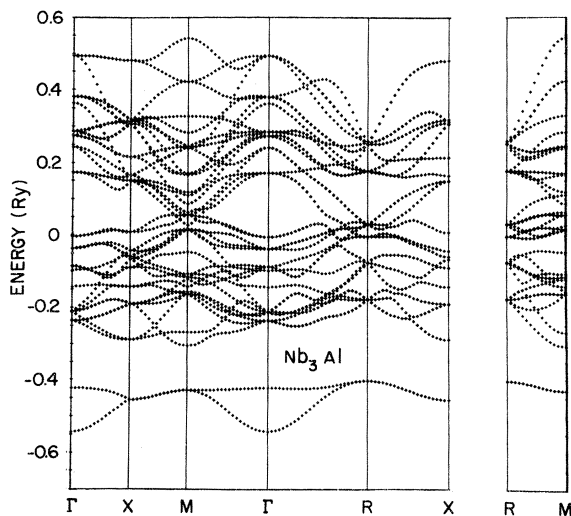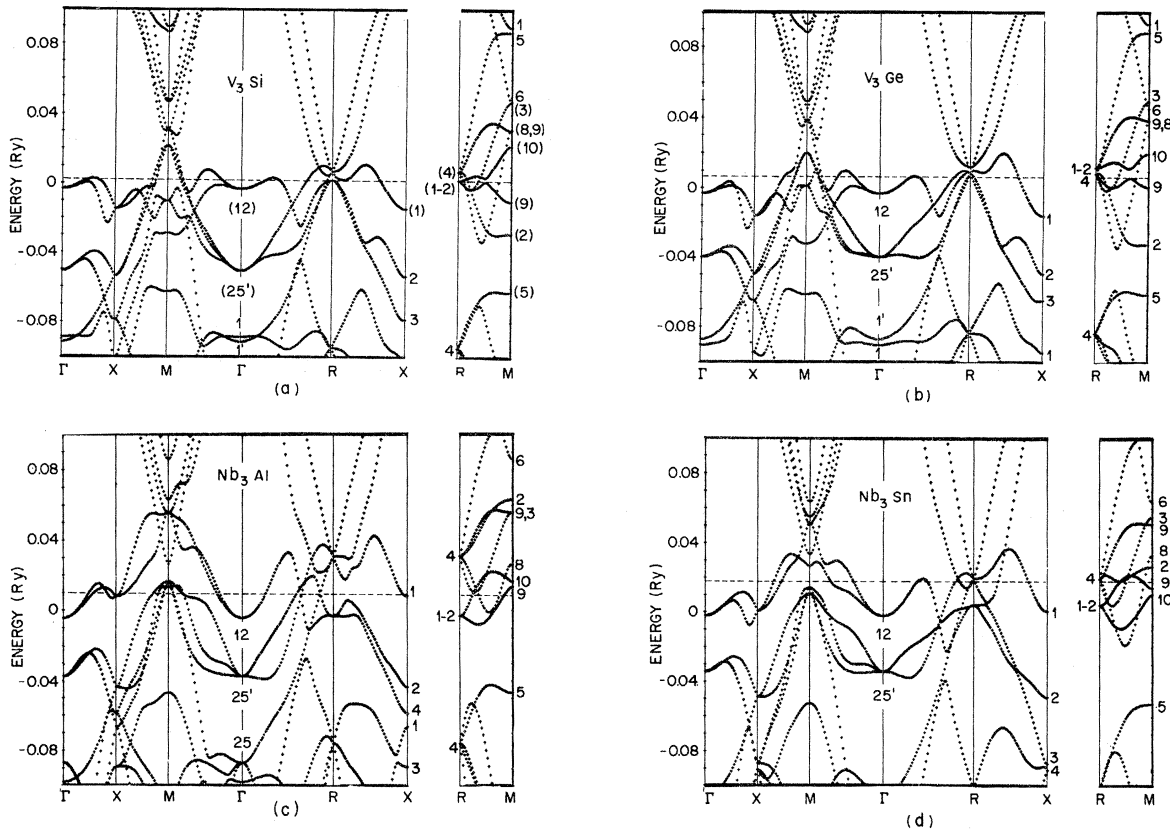

FIG. 4. APW-LCAO energy bands for Nb_3Al.

FIG. 6.　APW-LCAO energy bands near E_F for (a) V_3Si, (b) V_3Ge, (c) Nb_3Al, and (d) Nb_3Sn.

the complicated shapes of the band profiles near E_F are an artifact of the LCAO model (caused by fitting APW results only at symmetry points), or whether they truly reflect the APW bands along these symmetry lines. The LCAO fit to the X_1 state just below E_F is particularly poor. In each compound, it is found that the LCAO eigenvalue for this state is consistently above the APW result by about 0.015 Ry. It is believed that this error is due primarily to the effects of s-d hybridization, which are omitted in the present LCAO model.

Despite these uncertainties in the band shapes, it is clear from Fig. 6 that the bands below E_F tend to be relatively flat in comparison with those at higher energies. As a result, one expects a minimum in the density of states $N(E)$ slightly above the Fermi energy in these compounds. This feature is reflected in the $N(E)$ curves shown in Fig. 7. These results have been obtained by sampling $E(\vec{k})$ at 64 000 uniformly distributed points in the Brillouin zone (21 points along the ΓX line in Fig. 6, 1771 points in $\frac{1}{48}$ of the zone). Only minor changes are found in these curves when the number of sampling points is reduced to 32 768. These curves exhibit the gross features of the crude $N(E)$

curve for V_3Ga that is shown in Fig. 8 of I.

The detailed structure in $N(E)$ near E_F involves either a single relatively sharp peak (V_3Ge), a pair of such peaks (V_3Si and Nb_3Sn), or a cluster of smaller peaks (Nb_3Al). It seems likely that these differences in $N(E)$ near E_F reflect the basic limitations of the present APW-LCAO model in representing the band profiles along symmetry lines and at general points in the Brillouin zone. It will be necessary to extend the LCAO fit to APW results along symmetry lines in order to obtain a realistic estimate of the band-structure density of states near E_F in these $A15$ compounds.

Using the LCAO wave functions, one can also calculate the contribution of individual subbands to the total $N(E)$ curves for these compounds. In such a calculation, each LCAO eigenvalue is weighted by the sum of squares of the appropriate eigenvector coefficients. Since the present LCAO model involves orbital overlap, the appropriate weighting factor is the atomic population of Mulliken[27] in which the overlap charge is distributed equally among each pair of atoms. It turns out that these atomic populations are very similar in magnitude to the sum of squares of the eigenvectors of Löwdin's symmetric orthogonalization
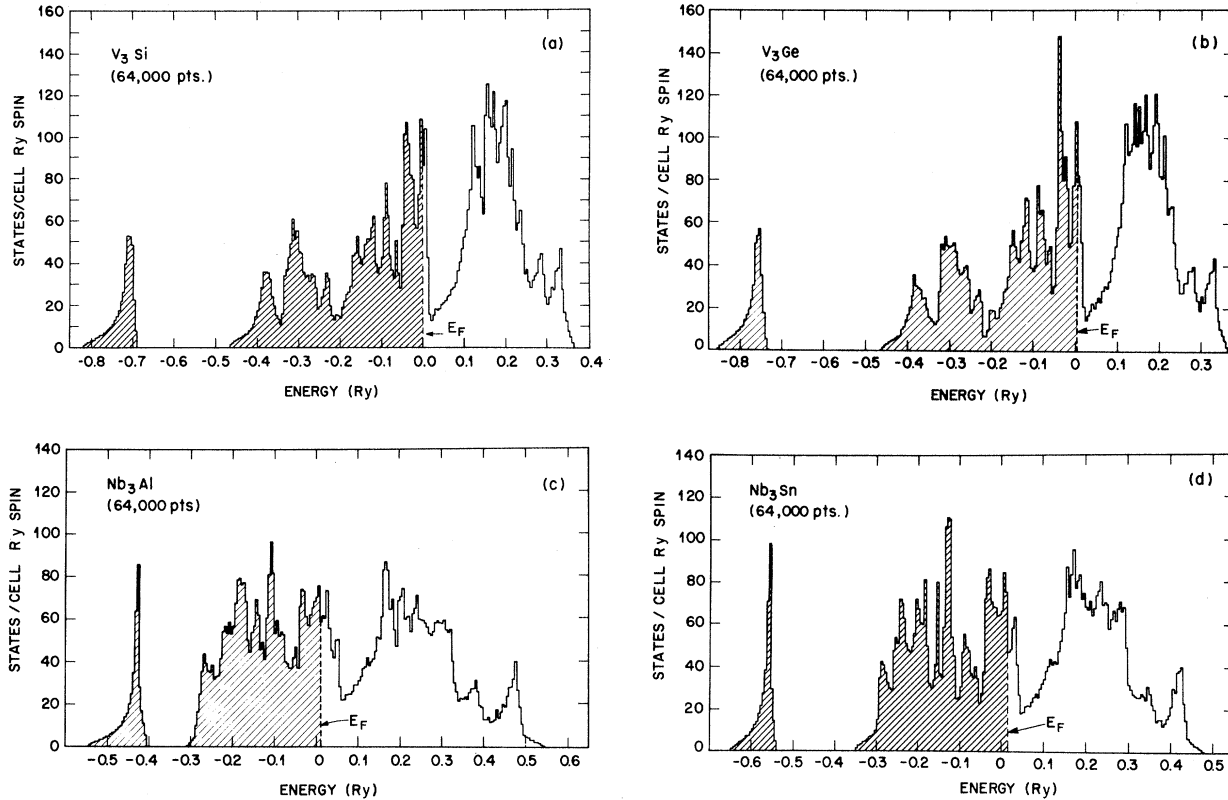
FIG. 7. $N(E)$ curves for (a) V_3Si, (b) V_3Ge, (c) Nb_3Al, and (d) Nb_3Sn.

scheme.[13,28]

This latter method has been applied to calculate the various subband contributions to $N(E)$ for V_3Si. These results are shown in Fig. 8. The top curve represents the total $N(E)$, while the lower curves reflect the π, σ, δ_2, δ_1, and p components, respectively. The A-atom s component is not shown, since $N_s(E)$ is always less than $(0.5$ states)/ (Ry spin cell) in this energy range. These curves involve the sampling of 32768 points in the Brillouin zone. A comparison of this total $N(E)$ curve with that in Fig. 7(a) illustrates the limited dependence of these curves on the number of sampling points.

Of particular interest is the symmetry of the energy-band states near E_F. The present LCAO model predicts that the largest contribution to $N(E)$ at E_F involves the δ_1 subband (43%). In decreasing order, the remaining contributions include the π (27%), $\delta_2(14\%)$, σ (13%), p (2%), and s (0.07%) components. These results emphasize the important differences between the present LCAO model and the IBA model of Weger and Goldberg,[2] where the δ_1 component of $N(E)$ is zero throughout the energy interval $E_F \pm 0.14$ Ry.

IV. BAND MODELS FOR THE A15 COMPOUNDS

A. Linear-chain model

The simplest band model for the A15 compounds is the linear-chain model of Labbé and Friedel.[5] As described in Sec. II C, this model neglects all interactions within the A-atom d manifold except those between nearest neighbors. In addition, it neglects all hybridization between the A- and B-atom s-p orbitals and the A-atom d-band states. These approximations produce three sets of one-dimensional d bands which are overlapped by a broad s-p band. Labbé and Friedel further assume that the Fermi level in the high-T_c materials lies within a few meV of a square-root singularity in $N(E)$.

The $E(\vec{k})$ curves for the linear-chain model d bands are shown in Fig. 9 for the two-center parameters $E_d = 0$, $(dd\sigma) = -0.20$ Ry, $(dd\pi) = 0.10$ Ry, and $(dd\delta) = -0.02$ Ry. The labels identify the various bands at symmetry points in the Brillouin zone. The corresponding labels for bands along symmetry lines can be determined from the compatibility relations. It is clear that this model predicts numerous accidental degeneracies at symmetry
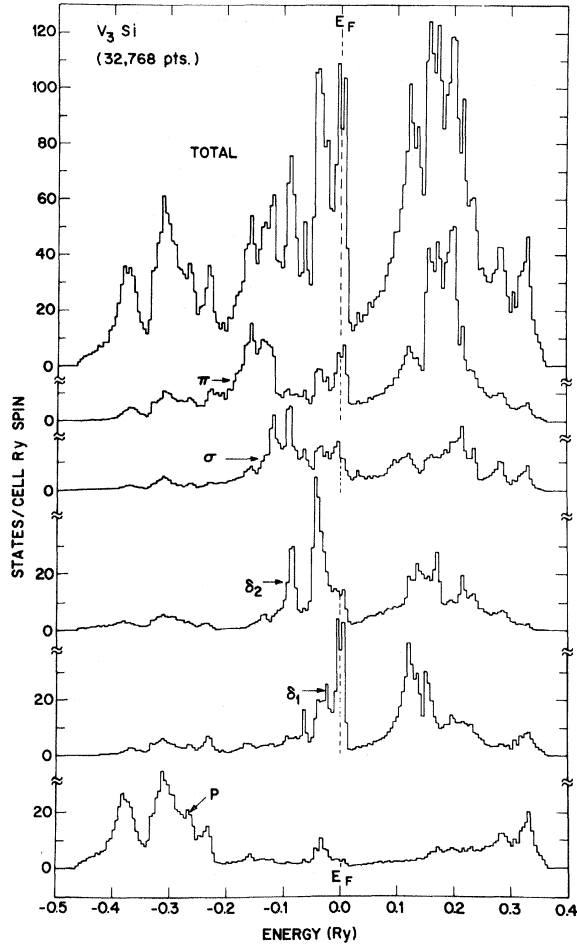
FIG. 8. Contributions of various subbands to $N(E)$ for V_3Si.

points and along symmetry lines. Those denoted by A, B, and C involve $\{X_1, X_1, X_2, X_3, X_4\}$, $\{R_1 - R_2, R_3, R_4, R_4, R_4, R_4\}$, and $\{M_1 - M_{10}, M_1, M_5, M_9, M_9, M_{10}\}$, respectively.

One can readily assess the validity of this linear-chain model by comparing the distribution of states at symmetry points with the APW-LCAO results in Figs. 2–5. It is found that all the accidental degeneracies of the linear-chain model are removed in these APW-LCAO results. An outstanding feature of the linear-chain model is the prediction that the d bandwidth is zero at R. Thus one can readily see from the APW-LCAO results in Figs. 2–5 that the corrections to the linear-chain model are about 0.3–0.4 Ry. Similar estimates of the strength of interchain $d-d$ interactions can be made at other points in the Brillouin zone. According to Table III, the states with $\Gamma_{1'}$ and $\Gamma_{12'}$ symmetry are pure d states. Their energy difference is due entirely to interchain $d-d$ interactions. According to the present APW results, these energy differences

are about 0.27 Ry in V_3Si and V_3Ge and 0.33 Ry in Nb_3Al and Nb_3Sn.

It is important to emphasize that the magnitude of these second-neighbor $d-d$ interactions in the $A15$ structure are typical of those found in similar studies for transition metals. For example, the second-neighbor Nb-Nb distance in Nb_3Sn is slightly smaller than that in bcc Nb. Pickett and Allen[29] have applied the Slater-Koster LCAO interpolation scheme to fit the results of APW calculations for bcc Nb. Expressed in two-center form, their second-neighbor $d-d$ interaction parameters are $(dd\sigma)_2 = -0.059$ Ry, $(dd\pi)_2 = -0.001$ Ry, and $(dd\delta)_2 = 0.004$ Ry. These are comparable with the second-neighbor LCAO parameters for Nb_3Sn in Table VII, where $(dd\sigma)_2 = -0.067$ Ry, $(dd\pi)_2 = 0.034$ Ry, and $(dd\delta)_2 = -0.008$ Ry. For nearest-neighbor $d-d$ interactions, Pickett and Allen obtain $(dd\sigma)_1 = -0.092$ Ry, $(dd\pi)_1 = 0.047$ Ry, and $(dd\delta)_1 = -0.003$ Ry, which also compare favorably with the nearest-neighbor parameters for Nb_3Sn in Table VII.

There is an additional factor that affects the accuracy of the linear-chain model. Namely, the relative contribution of any shell of neighbors to the A-atom d-band width is proportional to the product of the number of neighbors z_i times the strength of the interaction $E_{\alpha,\beta}(\vec{r}_i)$. In the bcc structure, the ratio of the number of second neighbors to nearest neighbors is 0.75, whereas this ratio is 4 in the $A15$ structure. This suggests that second-neighbor $d-d$ interactions could easily be more important in the $A15$ compounds than in the bcc metals.

B. Independent-band approximation

To correct these deficiencies in the linear-chain model, Weger and Goldberg[2] have extended this
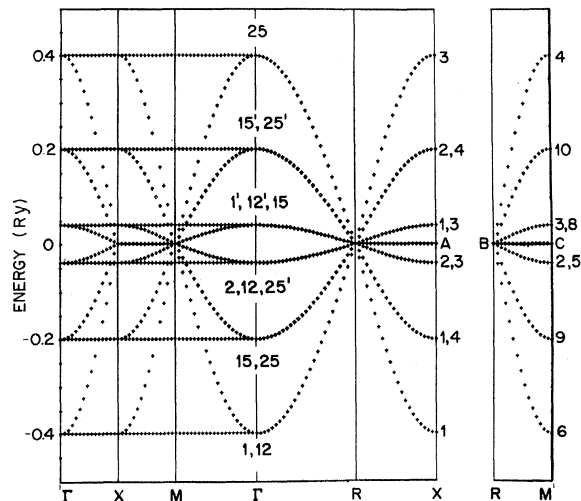
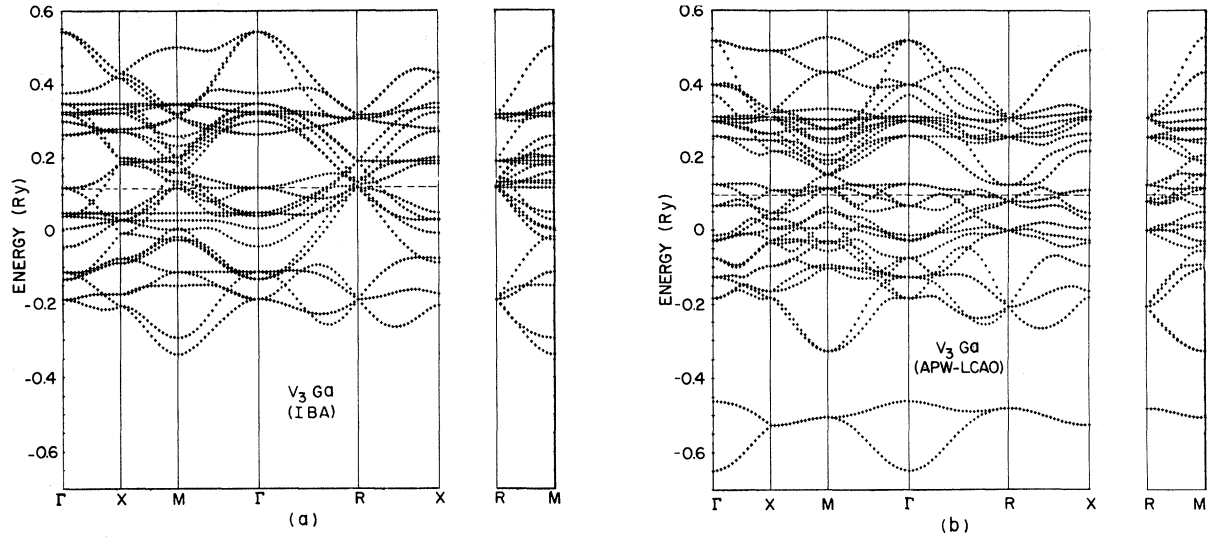

FIG. 9. $E(\vec{k})$ curves for the linear-chain model.

FIG. 10. Comparison between (a) the WG IBA and (b) present LCAO $E(\vec{k})$ curves for V_3Ga.

model to include limited coupling between the chains. As described in Sec. II C, this coupled-chain or IBA model omits all hybridization interactions between the σ, π, δ_1, and δ_2 subbands, and limits p-d interactions to the δ_1 subband. The Weger-Goldberg IBA $E(\vec{k})$ results for V_3Ga are shown in Fig. 10(a). They represent an optimized fit of the 22-parameter IBA model to the APW results for V_3Ga in Fig. 4 of I. For comparison, the $E(\vec{k})$ results of the present 21-parameter LCAO model for V_3Ga are shown in Fig. 10(b). In both cases, the energy scales are identical with that shown in Fig. 4 of I. It is noted that the present model includes the Ga $4s$ bands, whereas the IBA model does not.

The overall accuracy of the present LCAO model is such that the rms error is less than half that of the IBA. It is found that while the IBA yields 16 eigenvalues that differ from the APW results by more than 0.05 Ry, the present model yields only 2. The relative accuracy of these two tight-binding models can also be evaluated by examining the order of levels at symmetry points in the Brillouin zone. For example, the order of LCAO levels at Γ in Fig. 10(b) is identical with the APW results in I, whereas 10 out of 15 IBA levels are incorrectly ordered as a function of energy. Some of the more serious errors in the IBA model occur near E_F. At the zone center, the IBA model places a state with Γ_{15} symmetry at E_F, while the APW results in I and LCAO results in FIG. 10(b) involve a state with Γ_{12} symmetry. The corresponding Γ_{15} state is about 0.1 Ry above E_F in both the APW and LCAO results.

It is useful to compare the Weger-Goldberg IBA parameters for V_3Ga with those of the present

LCAO model. These results are contained in Table VIII. Let us consider first the results in the left-hand column. The IBA model neglects the Ga $4s$ bands $[E_s, (ss\sigma)_1, (ss\sigma)_2]$ and their overlap (S_s) and covalency $[(sd\sigma)]$ interactions with the V $3d$ states. It also neglects p-d overlap (S_σ and S_π). In the IBA model, p-d covalency interactions are restricted to those between p and δ_1-type d states. Values for the two-center parameters $(pd\sigma)$ and $(pd\pi)$ can be determined from these p-δ_1 IBA interaction parameters. [The Weger-Goldberg p-δ_1 matrix elements contain an extra factor of $\sqrt{2}$, which we absorb in the definitions of $(pd\sigma)$ and $(pd\pi)$ to allow direct comparison with the present LCAO values.] If we apply these IBA values for $(pd\sigma)$ and $(pd\pi)$ to estimate the p-d interaction integrals that are omitted in the IBA model, we obtain values for the p-σ, p-π, and p-δ_2 interaction integrals that are larger than those involving the p-δ_1 states. This result is confirmed by the present LCAO model in which $(pd\sigma)$ and $(pd\pi)$ are determined as an average over all p-d interactions.

Another interesting aspect of the IBA results in Table VIII concerns the "crystal-field" integrals $E_d(\sigma)$, $E_d(\pi)$, $E_d(\delta_1)$, and $E_d(\delta_2)$, respectively. These levels are distributed over an 0.29-Ry energy range in the IBA model. On the other hand, these "crystal-field" splittings are zero in the present LCAO model. It is believed[13] that these differences are due to the fact that the present LCAO model includes s-d and p-d orbital overlap.

We consider now the parameters in the right-hand column of Table VIII. The 20 LCAO entries involve only six independent two-center parameters. The omitted second-neighbor IBA parameters represent interband d-d hybridization inter-

TABLE VIII. Comparison between the Weger-Goldberg IBA and the present LCAO parameters for V_3Ga. The The LCAO $d-d$ interactions integrals $E_{\alpha,\beta}(\vec{\rho}_i)$ are evaluated in the two-center approximation, where $\vec{\rho}_1 = (0,0,\tfrac{1}{2})a$ and $\vec{\rho}_2 = (\tfrac{1}{4},\tfrac{1}{2},\tfrac{1}{4})a$.

Parameter	IBA	LCAO	Parameter[a]	IBA	LCAO
E_s	...	-0.508	$E_{3z^2,3z^2}(\vec{\rho}_1)$	-0.080	-0.071
$(ss\sigma)_1$	...	-0.013	$E_{yz,yz}(\vec{\rho}_1)$	0.070	0.087
$(ss\sigma)_2$	...	-0.006	$E_{xz,xz}(\vec{\rho}_1)$	0.095	0.087
E_p	-0.113	-0.014	$E_{xy,xy}(\vec{\rho}_1)$	-0.034	-0.030
$(pp\sigma)_1$	0.056	0.028	$E_{x^2,x^2}(\vec{\rho}_1)$	-0.005	-0.030
$(pp\pi)_1$	0.000	-0.011			
$(pp\sigma)_2$	0.018	0.022	$E_{xy,yz}(\vec{\rho}_2)$	-0.029	-0.027
$(pp\pi)_2$	0.009	-0.003	$E_{yz,yz}(\vec{\rho}_2)$	...	-0.004
$(sd\sigma)$	...	-0.073	$E_{zx,zx}(\vec{\rho}_2)$	...	-0.002
S_s	...	0.106	$E_{3z^2,yz}(\vec{\rho}_2)$	...	0.024
$(pd\sigma)$	-0.076	-0.021	$E_{x^2,yz}(\vec{\rho}_2)$	...	0.010
S_σ	...	0.247	$E_{yz,zx}(\vec{\rho}_2)$	-0.015	-0.002
$(pd\pi)$	0.152	0.067	$E_{zx,zx}(\vec{\rho}_2)$	0.001	-0.002
S_π	...	-0.014	$E_{3z^2,zx}(\vec{\rho}_2)$	...	0.012
			$E_{x^2,zx}(\vec{\rho}_2)$	...	0.021
$E_d(\sigma)$	0.187	0.128	$E_{yz,xy}(\vec{\rho}_2)$	-0.031	-0.027
$E_d(\pi)$	0.155	0.128	$E_{3z^2,xy}(\vec{\rho}_2)$	...	-0.003
$E_d(\delta_1)$	0.309	0.128	$E_{x^2,xy}(\vec{\rho}_2)$	...	0.026
$E_d(\delta_2)$	0.115	0.128	$E_{3z^2,3x^2}(\vec{\rho}_2)$	-0.003	-0.002
			$E_{x^2,3x^2}(\vec{\rho}_2)$	...	0.008
			$E_{x^2,y^2}(\vec{\rho}_2)$	0.010	-0.008

[a]An abbreviated notation replaces $3z^2 - r^2$, $x^2 - y^2$, $3x^2 - r^2$, and $y^2 - z^2$ by $3z^2$, x^2, $3x^2$, and y^2, respectively.

actions. It is found that the second-neighbor IBA intraband parameters agree well with those derived from the present LCAO model. However, it is clear from these results that interband $d-d$ interactions are not necessarily smaller than intraband interactions. Among the seven second-neighbor $d-d$ interaction parameters with magnitudes greater than 0.01 Ry, only two represent intraband interactions, whereas five involve interband interactions. Thus we conclude from the present analysis that the IBA approximation neglects off-diagonal interband matrix elements [proportional to $4E_{\alpha,\beta} \times (\vec{\rho}_2)$] that are at least 0.1 Ry in magnitude.

Weger and Goldberg obtain a similar estimate for these interband hybridization matrix elements. However, they claim that these matrix elements will have a small effect on the $E(\vec{k})$ and $N(E)$ curves since "the Van Hove peaks in the density of states appear to be due mostly to regions in the vicinity of high symmetry points." In fact, the two largest peaks in the IBA $N(E)$ curves in Fig. 45 of Ref. 2 coincide with δ_2 and σ bands (at energies of about 0.05 and 0.35 Ry) which are perfectly flat in the entire ΓXM plane. These flat bands and the

resulting peaks in $N(E)$ are the direct result of the IBA model which allows states of the same symmetry to "cross" without hybridization.

In order to explain the anomalous properties of the high-T_c A15 compounds, Weger and Goldberg shift the "crystal-field" parameters $E_d(\sigma)$, $E_d(\pi)$, and $E_d(\delta_2)$ by ± 0.05 Ry so as to place the large δ_2 peak in $N(E)$ at E_F. They justify these adjustments by estimating that the relative positions of the various subbands in the APW results in I are reliable only to about 0.1 Ry. They identify three sources of error, including nonspherical corrections inside the APW spheres, nonconstant corrections outside, and errors caused by lack of self-consistency in the potential. We have shown in Sec. II B that the effects of the first two corrections on the present APW results are small (~0.01 Ry). We present arguments in Sec. V which suggest that a self-consistent calculation will not alter appreciably the distribution of APW energy-band states near E_F in these A15 compounds.

In conclusion, there are serious discrepancies between the predictions of the Weger-Goldberg IBA model and the present LCAO model for the A15 compounds. The present LCAO model predicts that the peak in $N(E)$ near E_F is largely composed of states from the δ_1 subband (Fig. 8). The IBA model predicts a gap in the δ_1-p component of $N(E)$ such that there are no states from this subband within ± 0.14 Ry of E_F.

C. Coupled-band approximation

Goldberg[12] has extended the IBA model to include interband hybridization and $p-d$ interactions between the various d subbands in the A15 structure. In principle, this coupled-band approximation (CBA) is equivalent to the present LCAO model of Sec. II C. The main difference is that the CBA basis functions involve orthogonalized atomic orbitals, whereas the present LCAO model treats $s-d$ and $p-d$ orbital-overlap effects explicitly. In either model, the nonlinear least-squares fitting procedure can lead to spurious values for the LCAO parameters because of the highly nonlinear dependence of the energy levels on these parameters. As discussed in Sec. II D, these problems are minimized in the present study by first fitting the APW results by means of a simplified two-center approximation and then using these as starting values for the final parameter variations.

Goldberg, on the other hand, uses the IBA parameters as starting values for the CBA fit. In terms of 41 independent parameters, his CBA model fits the APW results for V_3Ga with an rms error of 0.025 Ry. However, Goldberg rejects these parameters as unphysical, because they differ significantly from the IBA starting values and fail to satisfy the two-center approximation. He ultimate-

ly chooses an alternative method for determining these parameters that involves a blend of fitted parameters plus "basic" integrals which are calculated using atomic wave functions. In the process, the rms error is increased to 0.046 Ry.

Using these parameters, Goldberg tests the IBA identification of APW levels at symmetry points in the Brillouin zone by means of the CBA wave functions. If the sum of squares of the σ, π, δ_1-p, or δ_2 components of a CBA eigenvector is greater (less) than 0.5, he describes the identification of that level as definite (indefinite). Using this criterion, he finds that the IBA identification of 73 V_3Ga APW levels is correct for 66, incorrect for 4, and indefinite for 3 levels. In terms of this same criterion, the corresponding results for the present LCAO model for V_3Ga are 49, 14, and 10. However, if one sharpens this criterion slightly by requiring that the square of the principal eigenvector component be greater than 0.67 rather than 0.5, then the number of indefinite states increases to 24.

These results demonstrate that interband hybridization is substantial in the A15 compounds, even at symmetry points in the Brillouin zone. Its effect on the IBA band structure is even more important along symmetry lines and at general points in the zone where the IBA allows accidental degeneracies and band crossings to occur. Consequently, it is not surprising that the CBA $N(E)$ curve for V_3Ga bears little resemblance to the IBA results. In particular, the two largest peaks in the IBA $N(E)$ curve disappear entirely in the CBA results. One of these is the IBA δ_2 peak that Weger and Goldberg shift in energy so as to place it at E_F in the high-T_c materials. Goldberg concedes that this peak is due to the δ_2 band that is perfectly flat in the ΓXM plane in the IBA model.

Goldberg finds that the V_3Ga Fermi level falls at a minimum in the density of states. He adjusts the relative energies of the various d subbands to produce a peak in $N(E)$ near E_F. However, his final band structure near E_F bears little to no resemblance to the original APW results for V_3Ga in I.

V. DISCUSSION AND INTERPRETATION

The highly simplified semiempirical models that have been applied to interpret the anomalous physical properties of the high-T_c A15 compounds involve fine structure in the density of states within a few meV of E_F. This degree of accuracy is certainly beyond the capabilities of current band-theoretical methods, particularly for materials with the complexity of the A15 compounds. Despite their limitations, first-principles band calculations can provide a useful frame of reference for evaluat-

ing the validity and limitations of various microscopic models that concentrate exclusively on such details in $N(E)$ near E_F.

We consider first the limitations of the present APW calculations for these A15 compounds and the manner in which semiempirical adjustments can be introduced into the LCAO model to minimize these deficiencies. The principal source of error in any band calculation lies in the crystal potential. Hopefully, these errors would be minimized if the potential were calculated self-consistently, though even here, errors would persist because of the approximate treatment of exchange and correlation effects. Both types of errors occur in the present calculations, which are not performed self-consistently. However, past experience has shown that these errors can be (at least partially) corrected by the empirical adjustment of a single LCAO parameter in the APW-LCAO band model.

In previous applications of this APW-LCAO model to transition-metal oxides with the ReO_3,[13] rock-salt,[14] and perovskite[15] structures, it has been found that the least reliable feature of the APW results is the energy separation between the oxygen $2s$-$2p$ and metal d bands. In the case of the oxides, potentials derived by superimposing atomic charge densities tend to overestimate this energy separation by about 0.2 Ry. More recent studies on transition-metal dichalcogenide layer compounds[30] yield a similar though somewhat smaller error of 0.05 Ry in the chalcogen-metal p-d band separation. Recent self-consistent APW calculations for[31] V_3Si suggest that similar errors occur in the present APW results for the A15 compounds.

Fortunately, the LCAO interpolation method provides a convenient framework for introducing semiempirical corrections to the APW results. However, in applying such corrections to materials with the complexity of the A15 structure, one must proceed with caution. As Phillips[32] emphasizes, semiempirical adjustments to a model Hamiltonian can be classified as arbitrary, inadvisable, or constructive. Semiempirical adjustments are not likely to be constructive unless the pertinent parameters in the model Hamiltonian have a fundamental rather than a numerical significance. As discussed in Secs. IIC and IID, the present LCAO interpolation scheme possesses important limitations in this respect because of the complexity of the A15 band structures.

An important example of these limitations is the "crystal-field" splittings of the d orbitals in V_3Ga in Table VIII. Here, we find an extreme situation, where the IBA model predicts crystal-field splittings of about 0.2 Ry between the centers of gravity of the various d subbands, whereas the two-center LCAO model yields a more accurate fit with
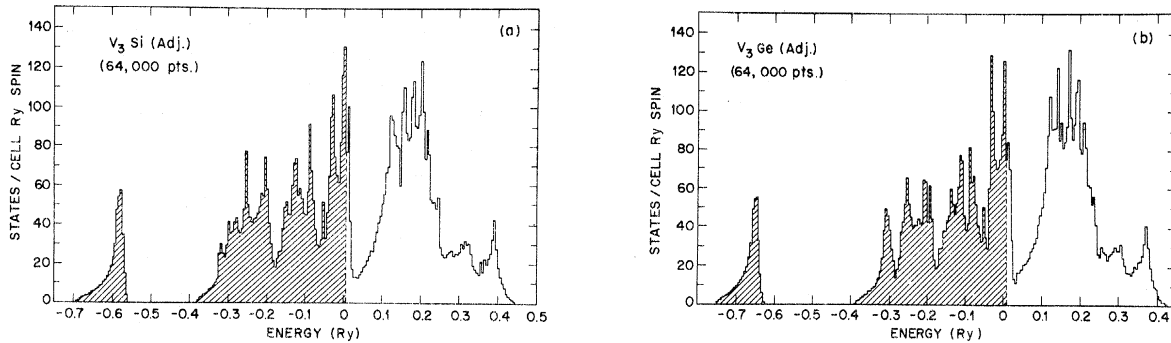
FIG. 11. $N(E)$ curves for the adjusted LCAO band structures of (a) V_3Si and (b) V_3Ge.

zero splitting. If the two-center approximation is relaxed in the latter model by allowing the E_d's to vary for the different subbands, one obtains a slight improvement in rms error (about 0.002 Ry) and crystal-field splittings of about 0.06 Ry. It is difficult to determine whether these splittings are fundamentally significant or whether they are merely numerical artifacts caused by adding three extra LCAO parameters.

Because of these uncertainties, we limit our semiempirical adjustments to a single parameter, the energy separation between E_d and the B-atom s-p orbital energies E_s and E_p. In the case of the $A15$ compounds, the most direct information about this energy separation is provided by the x-ray emission spectra of Nemnonov and Kurmaev.[33] These data indicate an occupied p-d valence bandwidth of about 6 eV for V_3Ga, V_3Si, V_3Ge, and Cr_3Si. This is in general agreement with the $N(E)$ curves for V_3Si and V_3Ge in Fig. 7. At lower energies, these data exhibit peaks at 6 eV (V_3Ga), 8 eV (V_3Si), and 9 eV (V_3Ge) below E_F which are due to the B-atom s bands. The present (and earlier) APW-LCAO results predict these peaks at 8 eV (Fig. 8 of I), 9.5 eV, and 10.3 eV below E_F, respectively. Thus, we conclude that these APW calculations overestimate the energy separation between the A-atom d bands and the B-atom s-p bands by about 1.5–2.0 eV.

We correct these deficiencies by reducing these energy separations in the LCAO model by 0.125 Ry (V_3Si) and 0.1 Ry (V_3Ge). The adjusted LCAO $N(E)$ curves for V_3Si and V_3Ge are shown in Fig. 11. If we compare these adjusted $N(E)$ curves with the original ones in Fig. 7, we find that although many of the gross features (such as the minimum at $E = 0.02$ Ry) survive, the detailed shape and height of the largest peaks can be substantially modified. In particular, the differences in the $N(E)$ peaks near E_F in Figs. 7 and 11 provide a realistic measure of the accuracy with which the present APW-LCAO band model can predict fine structure in $N(E)$.

Of course, it is possible to improve the resolution of the present $N(E)$ calculations by reducing the histogram width ($\Delta E = 0.005$ Ry) and utilizing the more elaborate techniques that are available for carrying out k-space integrations.[34] However, this added sophistication would be justified only if the intrinsic accuracy of the present LCAO model were also improved. As discussed in Sec. IIC, this would involve extending both the APW calculations and the LCAO fit to include energy-band states along symmetry lines in the Brillouin zone. To achieve sufficient accuracy, the LCAO model would probably require many additional parameters and also the inclusion of A-atom s-p orbitals in the LCAO basis.

A variety of spectroscopic methods have been applied to the $A15$ compounds in an effort to uncover fine structure in the valence-band density of states, including x-ray, ultraviolet photoemission, and optical studies. The resolution of the x-ray emission data[33] is such that it reveals only two or three broad peaks in the energy range of the A-atom d and the B-atom p bands. This is also the case for the x-ray emission spectra for Nb_3Sn by Hague and Bonnelle[35] and the ultraviolet photoemission spectra for V_3Si by Heiniger and Walldén.[36] Benda et al.[37] have sought evidence for fine structure in $N(E)$ near E_F in low-energy optical reflectivity data for V_3Si and V_3Ge. Their data for both compounds exhibit a minimum at 0.7 eV, a broad weak maximum near 1.1 eV, and a slowly decreasing reflectivity at the highest energies (3 eV). They tentatively attribute the reflectivity minimum at 0.7 eV to interband transitions.

To test this interpretation, we have calculated the joint density of states (JDOS) for direct transitions for the APW-LCAO band structures of Figs. 2–5. These JDOS curves are shown in Fig. 12. In agreement with the reflectivity data, we find that the JDOS curves for V_3Si and V_3Ge are virtually identical. Furthermore, the JDOS curves for
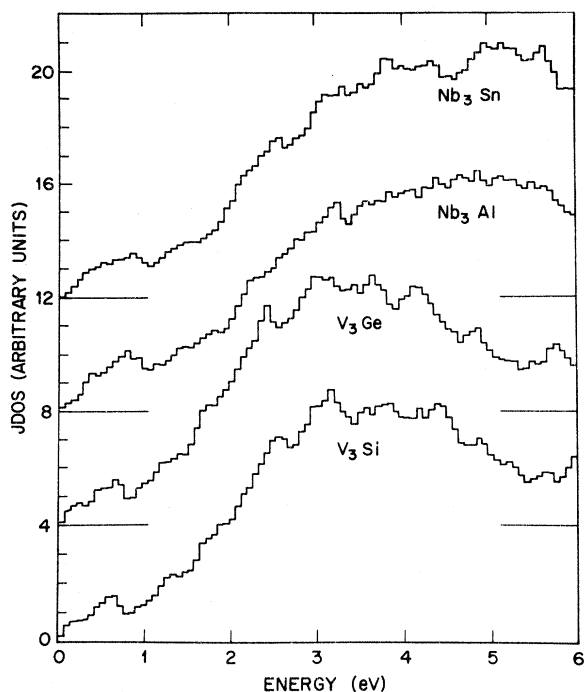
FIG. 12. Joint-density-of-states (JDOS) curves for direct transitions in the present A15 compounds.

both compounds exhibit a small peak near 0.7 eV. This peak is shifted to about 0.8 eV in Nb_3Al and Nb_3Sn. Although these JDOS results provide some support for the interpretation proposed by Benda et al.[37] for their optical data, it will be necessary to perform a Kramers-Kronig analysis of this data before a more rigorous interpretation is possible.

A limited amount of Fermi-surface data is available from positron-annihilation[38,39] and magneto-thermal oscillation[40] studies on single-crystal V_3Si and V_3Ge samples, respectively. The positron-annihilation studies were motivated largely by Weger's prediction[9] that the V_3Si band structure and Fermi surface are one-dimensional and that the latter consists of large, flat, nearly planar sections, oriented perpendicular to the $\langle 100 \rangle$ axes. These features would be readily observable as gross anisotropies in the orientation dependence of the positron-annihilation data. The initial studies by Mihalisin and Parks[38] exhibited no anisotropy differences in the $\langle 100 \rangle$ and $\langle 111 \rangle$ data. More recent measurements by Berko and Weger[39] have revealed small anisotropies in the $\langle 100 \rangle$, $\langle 110 \rangle$, and $\langle 111 \rangle$ data. While Mihalisin and Parks conclude that their results largely discredit Weger's linear-chain model, Berko and Weger claim that their data are consistent with the predictions of the linear-chain model.

In evaluating this situation, it is useful to com-

pare the anisotropy that is observed in the positron-annihilation data for V_3Si with that of a typical transition metal such as bcc V or Nb.[41] In the case of V_3Si, a plot of the difference between the normalized $\langle 100 \rangle$ and $\langle 111 \rangle$ data as a function of momentum yields a maximum anisotropy of 3%.[39] A similar plot of the analogous data for either bcc V or Nb contains anisotropies that are as large as 11%.[41] Consequently, we agree with the view of Mihalisin and Parks that second- and third-neighbor interactions lead to a much more isotropic band structure and Fermi surface for V_3Si than that predicted by Weger.[9]

The problem of inverting positron-annihilation data to obtain electron-momentum distributions and Fermi-surface topologies in metals and alloys is a complex one. Berko and Mader[42] have reviewed the progress that has been made thus far in this field. In general, this progress has been limited primarily to materials involving the simple and noble metals and their alloys, where the Fermi surface is nearly spherical. The present APW-LCAO band model predicts extremely complicated Fermi surfaces for the A15 compounds. The calculated Fermi surfaces for V_3Si and V_3Ge are shown in Fig. 13. Here, we plot the intersection of the various Fermi-surface sheets with the {100} and {110} symmetry planes of the cubic Brillouin zone. In both compounds, the Fermi-surface sheets involve primarily electrons in the 20th band (e_{20}) and holes in the 18th and 19th bands (h_{18} and h_{19}), each of which is cross-hatched differently. Neglecting the smaller hole pockets near M and R, the Fermi energy E_F is determined by the condition that the volume enclosed by e_{20} equals that of h_{18} plus h_{19}.

Of course, some details of these Fermi-surface results should be regarded as tentative because of the limited accuracy of the present LCAO interpolation method. Among the more reliable features is the fact that the bands that determine e_{20} are relatively flat, especially in comparison to those responsible for the hole pockets near M and R in the Brillouin zone. It is clear from Fig. 6 that this feature depends mainly on the APW results at symmetry points and the compatibility relations. As a result, we estimate that the cyclotron-mass ratios for electron orbits on e_{20} are 2–3 times larger than those for hole orbits on h_{19}, h_{18}, etc. Furthermore, this suggests that e_{20} provides the main contribution to $N(E_F)$ in these A15 compounds.

Predictions regarding the size, shape, and topology of the various Fermi-surface sheets involve greater uncertainties. For example, the closed electron sheets for V_3Si at Γ and X (e_{20}) would be connected by necks along Δ in Fig. 13(a) if the energy of the highest (Δ_2) band along the
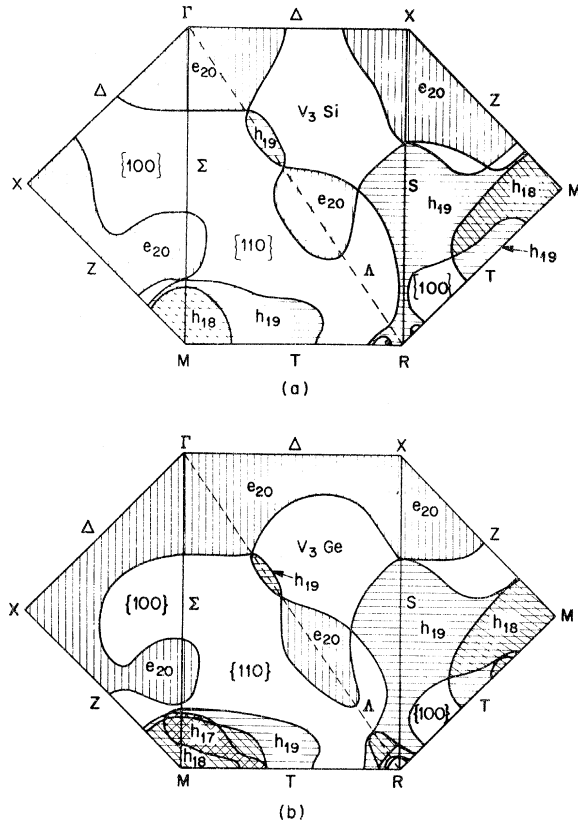
FIG. 13. Central {100} and {110} cross sections of the (a) V_3Si and (b) V_3Ge Fermi surfaces.

ΓX line in Fig. 6(a) were lowered by 0.002 Ry. The opposite would occur in V_3Ge if the Δ_1 band were raised by 0.003 Ry. Despite these uncertainties, the present LCAO model provides a realistic estimate of the degree of complexity that is expected for the Fermi surfaces of these $A15$ compounds.

Graebner and Kunzler[40] have observed three separate frequencies in their magnetothermal oscillation data for V_3Ge. From the angular dependence of these frequencies, they attribute them to extremal orbits on cylindrical-type surfaces with axes along the $\langle 100 \rangle$ directions. The present Fermi-surface model for V_3Ge includes a complex configuration of nested hole pockets at $M(h_{17}\cdots h_{19})$ and $R(h_{15}\cdots h_{19})$, all of which have reasonable cyclotron-mass ratios of about 1 or 2. However, as Graebner and Kunzler point out, the symmetry of the data rules out the latter possibility. Thus we tentatively assign these frequencies to the nested hole surfaces at M.

It is interesting to contrast these Fermi-surface results for V_3Si and V_3Ge with that predicted by the linear-chain model. The intersection of the d-band Fermi surface for this model with the sym-

metry planes of the Brillouin zone is shown in Fig. 14(a). Here, E_F is assumed to fall slightly above the flat δ bands at -0.04 Ry in Fig. 9. The shaded areas denote the various sheets of the δ-band Fermi surface. We ignore for the moment the complications that are caused by the π and σ sheets. A sketch of the δ-band Fermi surface is shown in Fig. 14(b). It consists of a total of six sheets; two identical sheets are denoted by α, two by β, and two by γ. This doubling of the δ-band Fermi surface results directly from the accidental degeneracy of the δ_1 and δ_2 subbands. The pair of γ sheets are determined by the intersection of three sets of planes which are perpendicular to the $\langle 100 \rangle$ axes and separated by W. The width W reduces to zero as E_F approaches the square-root singularity in $N(E)$ at $E = \pm 0.04$ Ry in Fig. 9. The pair of $\beta(\alpha)$ sheets correspond to the intersection of two (three) sets of mutually perpendicular planes of γ.

The topologies of the π-band and σ-band Fermi surfaces are identical to those of the δ subband. The dimension W in Fig. 14(b) is successively larger for the π and σ subbands. Each of these sheets (which are doubly and singly degenerate for the π and σ subbands, respectively) truncate the β and γ sheets of the δ-band Fermi surface. However, in this one-dimensional limit, electrons (or holes) are not scattered from one subband to another, so these truncations have no effect on the orbits of these carriers. A total of 15 Fermi-surface sheets are involved. They range from a pair of α-type electron pockets in the 15th band at Γ to a single γ-type hole pocket at R in the first
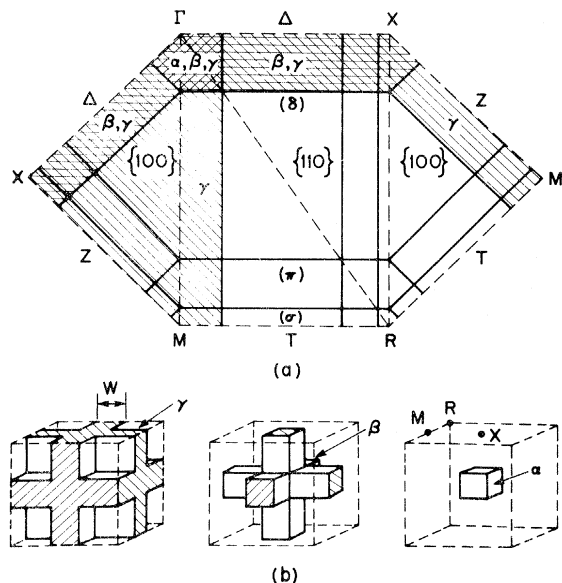

FIG. 14. Fermi surface of the d bands in the linear-chain approximation.

band.

If the corrections to this linear-chain band model were small, then their main effect on the Fermi surface of Fig. 14 would be restricted to regions of the Brillouin zone where accidental degeneracies occur. These would tend to round off the sharp edges of the various Fermi-surface sheets whenever crossings occur in Fig. 14(a). The result would be a complicated array of 15 nearly planar Fermi-surface sheets with slightly rounded corners and edges. These effects would smear the square-root singularity in $N(E)$. It is clear that the present APW-LCAO Fermi-surface results for V_3Si and V_3Ge in Fig. 13 contain few if any features of this linear-chain model.

Values for $N(E_F)$ in the A15 compounds have been estimated from specific-heat and super-conductivity data using the McMillan formula.[7] However, Testardi[1] has shown that, because of the structural instability of the high-T_c materials, the standard interpretation of specific-heat data is probably incorrect. In particular, a calculation of the lattice specific heat for V_3Si reveals a term nearly linear in temperature. As a result, the extrapolation of specific-heat data from above T_c to 0 °K yields a sum of both electronic and lattice contributions, rather than the electronic term alone. Another difficulty is the fact that this extrapolation must span a large temperature range in the high-T_c materials.

Numerous specific-heat studies have been carried out on these compounds. In both V_3Si and Nb_3Sn, the recent estimates[43] for γ are (20–30)% smaller than the earliest values.[44] Smaller variations [(5–10)%] are found in the corresponding results for[45] V_3Ge and Nb_3Al. Junod[43] has determined the band-structure $N(E_F)$ and the phonon-enhancement factor λ for V_3Si, Nb_3Al, and Nb_3Sn, using the McMillan formula. He obtains the values $N(E_F)$ = 1.6 (V_3Si), 1.1 (Nb_3Al), and 1.5 (Nb_3Sn) in units states/(eV spin A-atom), with $\lambda(V_3Si)$ = 1.3, $\lambda(Nb_3Al)$ = 1.1, and $\lambda(Nb_3Sn)$ = 1.4. These values for Nb_3Al agree with those of Willens et $al.$[46] Using earlier data, McMillan[7] estimated $N(E_F)$ = 2.4 and λ = 0.8 for V_3Si in these same units. Assuming $\lambda(V_3Ge)$ ≈ 1, the specific-heat data for V_3Ge yield[44] $N(E_F)$ = 1.1. The present APW-LCAO band model predicts values for $N(E_F)$ = 1.1 (V_3Si), 1.0 (V_3Ge), 0.7 (Nb_3Al), and 0.6 (Nb_3Sn), respectively. The agreement between these theoretical and experimental values is considered satisfactory in view of the limited accuracy of the present LCAO model.

It appears that the major discrepancy between the present $N(E)$ results and those of the more simplified models[4–6] concerns the rapid variations in $N(E)$ near E_F as E increased by a few meV. This would require bands near E_F whose curvature and width are reduced by about two orders of mag-

nitude from that shown in Fig. 6, particularly for the "anomalous" compounds, V_3Si and Nb_3Sn. Unfortunately, it would be necessary to improve the accuracy of the present APW-LCAO model by two orders of magnitude before one could even attempt to resolve this question in terms of a first-principles calculation.

Independent estimates of $N(E_F)$ in these compounds have been obtained from nuclear-resonance studies. Fradin and Williamson[47] have applied spin-lattice relaxation rate and quadrupole interaction data for $V_3Ga_{1-x}Si_x$ alloys to determine the various subband contributions to $N(E)$ at E_F. In V_3Si, they find that the π subband is the major component (63%) of $N(E_F)$ = 2.6 states/(eV spin V-atom). Unfortunately, their analysis of these data relies heavily on the Weger-Goldberg $N(E)$ curves for V_3Ga. In particular, they assume that the δ_1 component of $N(E)$ is zero for V_3Si and that the main contribution to $N(E_F)$ involves the π and δ_2 subbands. A similar difficulty occurs in the interpretation of nuclear-acoustic-resonance data by Buttet and Laüger,[48] which involves wave functions derived from a linear-chain approximation to the Weger-Goldberg IBA model. Finally, from Knight-shift and relaxation-time measurements on several Nb_3X compounds, Ehrenfreund et $al.$[49] estimate an upper limit to the Nb 5s component of $N(E_F)$ in these compounds to be about 0.07 states/(eV spin Nb-atom), or about 5% of the total $N(E_f)$. This is consistent with the present APW-LCAO model, where it is assumed that the bottom of the A-atom s bands lies several eV above E_F. This is not the case in the Weger-Goldberg IBA or the Labbé-Friedel linear-chain models.

In summary, the present APW-LCAO band model for the A15 compounds predicts a peak in $N(E)$ near E_F that consists mainly of states derived from the δ_1 subband of the A-atom d manifold. It will be necessary to improve the accuracy of this model by about two orders of magnitude in order provide realistic first-principles estimates of the detailed shape and height of $N(E)$ near E_F in these materials. Despite these limitations, the present results raise serious questions regarding the existence of one-dimensional or quasi-one-dimensional features in the electronic structure of the A15 compounds.

ACKNOWLEDGMENTS

Traum, and W. A. Reed. I also wish to acknowl-edge interesting conversations with S. Berko con-cerning positron-annihilation data and their inter-pretation.

[1]L. R. Testardi, in *Physical Acoustics*, edited by W. P. Mason and R. N. Thurston (Academic, New York, 1973), Vol. X.

[2]M. Weger and I. B. Goldberg, in *Solid State Physics*, edited by H. Ehrenreich, F. Seitz, and D. Turnbull (Academic, New York, 1973), Vol. 28.

[3]C. M. Varma, J. C. Phillips, and S.-T. Chui, Phys. Rev. Lett. 33, 1223 (1974).

[4]A. M. Clogston and V. Jaccarino, Phys. Rev. 121, 1357 (1961).

[5]J. Labbé and J. Friedel, J. Phys. Radium 27, 153 (1966).

[6]R. W. Cohen, G. D. Cody, and J. J. Halloran, Phys. Rev. Lett. 19, 840 (1967).

[7]W. L. McMillan, Phys. Rev. 167, 331 (1968).

[8]L. R. Testardi, Phys. Rev. B 5, 4342 (1972).

[9]M. Weger, Rev. Mod. Phys. 36, 175 (1964).

[10]L. F. Mattheiss, Phys. Rev. 138, A112 (1965).

[11]J. C. Slater and G. F. Koster, Phys. Rev. 94, 1498 (1954).

[12]I. B. Goldberg, J. Phys. C 8, 1159 (1975).

[13]L. F. Mattheiss, Phys. Rev. 181, 987 (1969); B 2, 3918 (1970).

[14]L. F. Mattheiss, Phys. Rev. B 5, 290 (1972); 5, 306 (1972).

[15]L. F. Mattheiss, Phys. Rev. B 6, 4718 (1972); 6, 4740 (1972).

[16]W. Gorzkowski, Phys. Status Solidi 3, 910 (1963).

[17]L. F. Mattheiss, Solid State and Molecular Theory Group Quarterly Progress Report (M.I.T.) 51, 54 (1964) (unpublished).

[18]L. P. Bouckaert, R. Smoluchowski, and E. Wigner, Phys. Rev. 50, 58 (1936).

[19]B. W. Batterman and C. S. Barrett, Phys. Rev. Lett. 13, 390 (1964); Phys. Rev. 149, 296 (1966).

[20]R. Mailfert, B. W. Batterman, and J. J. Hanak, Phys. Lett. A 24, 315 (1967); Phys. Status Solidi A 32, K67 (1969).

[21]G. Shirane and J. D. Axe, Phys. Rev. B 4, 2957 (1971).

[22]L. F. Mattheiss, J. H. Wood, and A. C. Switendick, in *Methods in Computational Physics*, edited by B. Alder, S. Fernbach, and M. Rotenberg (Academic, New York, 1968), Vol. 8.

[23]F. Herman and S. Skillman, *Atomic Structural Calculations* (Prentice-Hall, Englewood Cliffs, N. J., 1963).

[24]L. Hodges, H. Ehrenreich, and N. D. Lang, Phys. Rev. 152, 505 (1966); F. M. Mueller, Phys. Rev. 153, 659 (1967); N. V. Smith and L. F. Mattheiss, Phys. Rev. B 9, 1341 (1974).

[25]Because of an oversight, we have assumed that
$E_{xy,yz}(\vec{r}_3 - \vec{r}_5) = E_{yz,xz}(\vec{r}_3 - \vec{r}_5)$ and $E_{xy,zx}(\vec{r}_3 - \vec{r}_5)$
$= E_{yz,zx}(\vec{r}_3 - \vec{r}_5)$, thereby reducing the number of second-neighbor parameters from 15 to 13. Removing this re-striction reduces the rms error by 0.001 Ry.

[26]A complete tabulation of the APW results and the cor-responding LCAO parameters is available from the author on request.

[27]R. S. Mulliken, J. Chem. Phys. 23, 1833 (1955).

[28]P. O. Löwdin, J. Chem. Phys. 18, 365 (1950).

[29]W. E. Pickett and P. B. Allen, Phys. Lett. A 48, 91 (1974).

[30]L. F. Mattheiss, Phys. Rev. B 8, 3719 (1973).

[31]B. M. Klein, D. A. Papaconstantopoulos, and L. F. Mattheiss, Bull. Am. Phys. Soc. 20, 297 (1975).

[32]J. C. Phillips, Adv. Phys. 17, 79 (1968).

[33]S. A. Nemnonov and E. Z. Kurmaev, Phys. Status Solidi A 24, K43 (1967); 43, K49 (1971); S. A. Nem-nonov, E. Z. Kurmaev, and V. P. Belash, *ibid.* 39, 39 (1970).

[34]F. M. Mueller, in *Computational Methods in Band Theory*, edited by P. M. Marcus, J. F. Janak, and A. R. Williams (Plenum, New York, 1971).

[35]C. F. Hague and C. Bonnelle, in *Band Structure Spec-troscopy of Metals and Alloys*, edited by D. J. Fabian and L. M. Watson (Academic, London, 1973).

[36]F. Heiniger and L. Walldén, Phys. Status Solidi A 5, 75 (1971).

[37]J. A. Benda, T. H. Geballe, and J. H. Wernick, Phys. Lett. A 46, 389 (1974).

[38]T. W. Mihalisin and R. D. Parks, in *Low Temperature Physics*, LT9, edited by J. B. Daunt, D. O. Edwards, F. J. Milford, and M. Yaqub (Plenum, New York, 1965).

[39]S. Berko and M. Weger, Phys. Rev. Lett. 24, 55 (1970); in *Computational Solid State Physics*, edited by F. Herman, N. W. Dalton, and T. R. Koehler (Plenum, New York, 1972).

[40]J. E. Graebner and J. E. Kunzler, J. Low Temp. Phys. 1, 443 (1969).

[41]N. Shiotani, T. Okada, T. Mizoguchi, and H. Sekizawa, J. Phys. Soc. Jpn. 38, (1975).

[42]S. Berko and J. Mader, Appl. Phys. 5, 287 (1975).

[43]A. Junod, Ph.D. thesis (University of Geneva, 1974) (unpublished).

[44]F. J. Morin and J. P. Maita, Phys. Rev. 129, 1115 (1963).

[45]These references are available in Refs. 1 and 2.

[46]R. H. Willens, T. H. Geballe, A. C. Gossard, J. P. Maita, A. Menth, G. W. Hull, Jr., and R. R. Soden, Solid State Commun. 7, 837 (1969).

[47]F. Y. Fradin and J. D. Williamson, Phys. Rev. B 10, 2803 (1974).

[48]J. Buttet and K. Laüger, Phys. Rev. B 9, 4643 (1974).

[49]E. Ehrenfreund, A. C. Gossard, and J. H. Wernick, Phys. Rev. B 4, 2906 (1971).